

## **Dual-excitation Ratiometric NIR-II fluorescent Nanoplatform Enables High Contrast In Vivo Imaging**

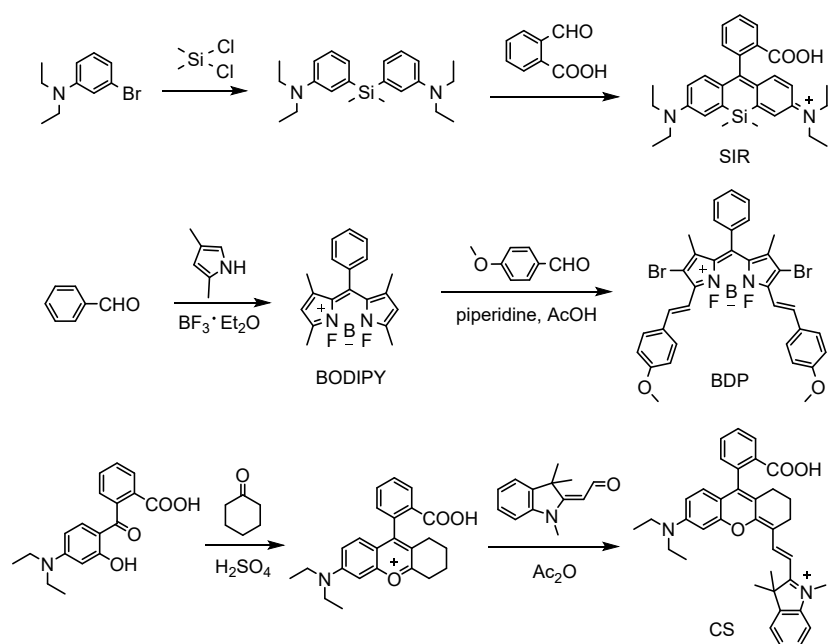
Yongchao Liu<sup>a,b\*</sup>, Lili Teng<sup>a</sup>, Bo Zhang<sup>a</sup>, Xiao-Bing Zhang<sup>b</sup> and Guosheng Song<sup>b\*</sup>

- a. State Key Laboratory of New Pharmaceutical Preparations and Excipients, Key Laboratory of Medicinal Chemistry and Molecular Diagnosis of Ministry of Education, College of Chemistry and Materials Science, Hebei University, Baoding, 071002. China.*
- b. State Key Laboratory of Chemo/Biosensing and Chemometrics, College of Chemistry and Chemical Engineering, Hunan University, Changsha, 410082. China.*

## Materials and characterization

All chemicals and reagents were purchased from commercial suppliers and used without further purification. DMEM, FBS, and penicillin-streptomycin were purchased from Gibco, Life Technologies. Mice were purchased from Hunan Slake Jingda Laboratory Animal Co., Ltd. Thin layer chromatography (TLC) was conducted using silica gel 60 F254, and column chromatography was carried out over silica gel (200-300 mesh) obtained from Qingdao Ocean Chemicals (Qingdao, China). Mass spectra were performed using an LCQ Advantage ion trap mass spectrometer (Thermo Finnigan). NMR spectra were recorded on a Bruker DRX-400 spectrometer using TMS as an internal standard. Transmission electron microscope images were accomplished using a JEM-2100 instrument (JEOL). Dynamic light scattering (DLS) measurements were made on a Malvern Zetasizer Nano ZS90 (Malvern). Water was purified and doubly distilled by a Milli-Q system (Millipore, USA). UV-Visible absorption spectra were acquired *via* the Shimadzu UV-2600 UV-VIS-NIR spectrophotometer. NIR-I fluorescence spectra were recorded on a spectrofluorometer (HITACHI F7000) and NIR-II fluorescence spectra were recorded on a spectrofluorometer (Edinburgh Instrument-FS5) with a 1 cm standard quartz cell.

The synthesis of SIR, BDP, CS and BBT-NO<sub>2</sub> was performed according to the literature<sup>1-4</sup>. The synthetic route is shown in Scheme S1.



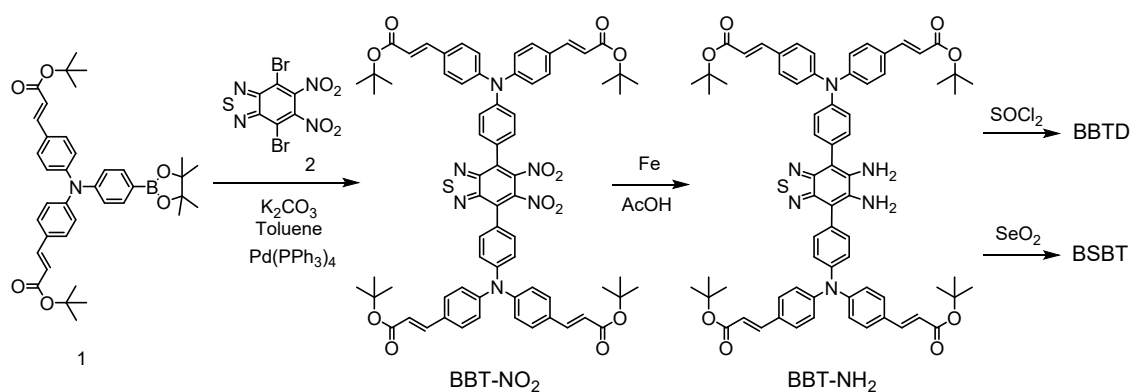
**Scheme S1.** The synthetic route of SIR, BDP, and CS.

**Synthesis of SIR.** The synthesis of SIR was performed according to the literature<sup>1</sup>. <sup>1</sup>H NMR (400 MHz, CDCl<sub>3</sub>)  $\delta$  = 7.96 (1 H, d, J=7.6), 7.64 (1 H, d, J=7.4), 7.56 (1 H, d, J=7.6), 7.35 (1 H, d, J=7.7), 6.91 (2 H, d, J=2.8), 6.71 (2 H, d, J=8.9), 6.47 (2 H, dd, J=8.9, 2.8), 3.35 (8 H, q, J=7.1), 1.14 (12 H, t, J=7.0), 0.61 (6 H, d, J=8.3). <sup>13</sup>C NMR (101 MHz, CDCl<sub>3</sub>)  $\delta$  = 170.66, 154.18, 146.58, 137.28, 134.03, 133.48, 130.80, 129.06, 128.53, 125.77, 125.53, 124.84, 115.94, 112.45, 44.26, 12.57, 0.44, -1.76.

**Synthesis of BDP.** The synthesis of BDP was performed according to the literature<sup>2</sup>. <sup>1</sup>H NMR (400 MHz, CDCl<sub>3</sub>)  $\delta$  = 7.64 (1 H, s), 7.59 (5 H, d, J=8.5), 7.49 (3 H, s), 7.34 (2 H, s), 7.21 (2 H, d, J=16.2), 6.93 (4 H, d, J=8.3), 6.61 (2 H, s), 3.86 (6 H, s), 1.43 (6 H, s). <sup>13</sup>C NMR (151 MHz, CDCl<sub>3</sub>)  $\delta$  = 160.40, 152.72, 141.78, 135.73, 135.32, 129.60, 129.05, 129.03, 128.88, 128.55, 117.50, 117.29, 114.28, 55.39, 14.60.

**Synthesis of CS.** The synthesis of CS was performed according to the

literature<sup>3</sup>. <sup>1</sup>H NMR (400 MHz, *d*<sub>6</sub>-DMSO)  $\delta$  = 12.79 (1H, s), 8.56 (1H, d, *J* = 14.2 Hz), 8.15 (1H, dd, *J* = 7.8, 0.8 Hz), 7.80 (1H, td, *J* = 7.5, 1.2 Hz), 7.69 (2H, dd, *J* = 12.6, 4.5 Hz), 7.50-7.43 (2H, m), 7.31 (2H, dd, *J* = 9.3, 4.5 Hz), 6.81 (1H, dd, *J* = 9.2, 2.4 Hz), 6.70 (1H, d, *J* = 2.3 Hz), 6.62 (1H, d, *J* = 9.1 Hz), 6.27 (1H, d, *J* = 14.1 Hz), 3.73 (3H, s), 3.53 (4H, q, *J* = 7.0 Hz), 2.66 (2H, t, *J* = 5.6 Hz), 2.34-2.16 (2H, m), 1.74 (8H, t, *J* = 14.2 Hz), 1.18 (6H, t, *J* = 7.0 Hz). <sup>13</sup>C NMR (101 MHz, *d*<sub>6</sub>-DMSO)  $\delta$  = 174.43, 172.47, 167.17, 162.19, 155.47, 151.75, 151.23, 143.25, 141.45, 135.66, 133.31, 131.21, 130.75, 129.95, 129.83, 129.00, 128.16, 125.72, 122.89, 120.60, 114.84, 113.07, 112.54, 111.96, 96.06, 55.37, 49.55, 44.82, 32.08, 28.18, 26.78, 21.52, 20.56, 12.80.



**Scheme S2.** The synthetic route of BBT-D and BSBT.

**Synthesis of BBT-NO<sub>2</sub>.** The synthesis of CS was performed according to the literature<sup>4</sup>. Compound 1 (1.25 g, 2 mmol), compound 2 (383 mg, 1 mmol), Pd(PPh<sub>3</sub>)<sub>4</sub> (115 mg, 0.1 mmol), and aqueous K<sub>2</sub>CO<sub>3</sub> (2 M, 2 mL) in toluene (30 mL) was bubbled with N<sub>2</sub> for 10 min. The mixture was heated in an oil bath at 120 °C for 48 hours. The reaction was allowed to cool to room temperature and extracted with EtOAc. The combined organic layers were washed with water (100 mL) and saturated brine solution (100 mL). After drying over anhydrous Na<sub>2</sub>SO<sub>4</sub> and removal of the solvents under reduced pressure, the residue was purified by column chromatography on silica gel with petroleum ether and EtOAc as eluent to yield **BBT-NO<sub>2</sub>** (252 mg, 21%

yield).  $^1\text{H}$  NMR (400 MHz,  $\text{CDCl}_3$ )  $\delta$  = 7.56 (4H, d,  $J=15.9$  Hz), 7.48 (12H, t,  $J=7.7$  Hz), 7.27-7.22 (4H, m), 7.17 (8H, d,  $J=8.0$  Hz), 6.30 (4H, d,  $J=16.1$ ), 1.54 (36H, s).  $^{13}\text{C}$  NMR (101 MHz,  $\text{CDCl}_3$ )  $\delta$  = 166.45, 153.07, 148.59, 147.85, 142.51, 130.57, 129.40, 129.16, 127.95, 124.98, 124.54, 124.04, 123.24, 119.25, 80.50, 28.24.

**Synthesis of BBT-NH<sub>2</sub>.** To a 10 mL sealed tube was added BBT-NO<sub>2</sub> (253 mg, 0.2 mmol), iron powder (112 mg, 2 mmol), and AcOH (10 mL). The reaction mixture was heated to 100 °C for 6 h and then cooled to room temperature. The reaction was neutralized with saturated sodium bicarbonate solution and extracted with EtOAc. The combined organic layers were washed with water (50 mL), dried over anhydrous Na<sub>2</sub>SO<sub>4</sub> and evaporated in vacuo. The residue was purified by recrystallization from petroleum ether and ethyl acetate to obtain **BBT-NH<sub>2</sub>**.  $^1\text{H}$  NMR (400 MHz,  $\text{CDCl}_3$ )  $\delta$  = 7.82 (8H, d,  $J=11.3$  Hz), 7.70 (10H, s), 7.58 (6H, s), 7.45 (8H, d,  $J=7.0$  Hz), 6.56 (4H, d,  $J=15.7$  Hz), 4.02 (2H, s), 1.81 (36H, s).  $^{13}\text{C}$  NMR (101 MHz,  $\text{CDCl}_3$ )  $\delta$  = 166.87, 151.30, 148.75, 143.08, 138.50, 131.75, 130.48, 129.91, 129.54, 125.53, 124.38, 118.88, 113.46, 80.69, 28.52.

**Synthesis of BBTD.** Compound **BBT-NH<sub>2</sub>** (116 mg, 0.1 mmol), SOCl<sub>2</sub> (60 mg, 0.5 mmol), DIPEA (129 mg, 1 mmol) were dissolved in anhydrous THF (10 mL) and stirred at 65 °C for 10 h under N<sub>2</sub> atmosphere in a two-neck flask, followed by evaporation of the solvent under reduced pressure. The residue was purified by column chromatography on silica gel with petroleum ether and dichloromethane as eluent to yield **BBTD** (25 mg).  $^1\text{H}$  NMR (400 MHz,  $\text{CDCl}_3$ )  $\delta$  = 8.27 (4 H, d,  $J=8.2$ ), 7.56 (4 H, d,  $J=15.9$ ), 7.46 (8 H, d,  $J=8.1$ ), 7.36 (4 H, d,  $J=8.0$ ), 7.22 (8 H, d,  $J=8.1$ ), 6.30 (4 H, d,  $J=15.9$ ), 1.54 (36 H, s).  $^{13}\text{C}$  NMR (101 MHz,  $\text{CDCl}_3$ )  $\delta$  = 166.55, 152.76, 148.29, 147.10, 142.76, 133.13,

130.42, 130.01, 129.32, 124.55, 123.89, 120.25, 118.83, 80.43, 28.25.

**Synthesis of BSBT.** Compound **BBT-NH<sub>2</sub>** (66 mg, 0.05 mmol) and selenium dioxide (55 mg, 0.5 mmol) were dissolved in EtOH (10 mL) and stirred at room temperature for 12 h, followed by evaporation of the solvent under reduced pressure. The residue was purified by column chromatography on silica gel with petroleum ether and dichloromethane as eluent to yield **BSBT** as a bottle green solid (12 mg). <sup>1</sup>H NMR (400 MHz, CDCl<sub>3</sub>) δ = 8.18 (4H, d, J=8.6), 7.56 (4H, d, J=15.9), 7.46 (8H, d, J=8.6), 7.34 (4H, d, J=8.7), 7.22 (8H, d, J=8.5), 6.30 (4H, d, J=15.9), 1.51 (36H, s). <sup>13</sup>C NMR (101 MHz, CDCl<sub>3</sub>) δ = 166.54, 152.78, 148.31, 146.91, 142.76, 133.35, 131.23, 129.95, 129.29, 125.08, 124.52, 123.78, 118.79, 80.42, 28.25. MALDI-MS (ESI) Calcd for: C<sub>70</sub>H<sub>68</sub>N<sub>6</sub>O<sub>8</sub>SSe<sup>+</sup> ([M+H]<sup>+</sup>): 1233.41. Found: 1232.809.

**Preparation of DERF-NPs.** For preparation of DERF-NPs, a mixed tetrahydrofuran (THF) solution (2 mL) containing SIR or BDP or CS (100 μg), PSMA (0.5 mg), BBTD or BSBT (100 μg), and Pluronic F127 (20 mg) was rapidly injected into distilled-deionized water (10 mL) under sonication. After sonication for another 10 min, the solution was evaporated at 50 °C by rotary evaporation to remove excess THF. Finally, the DERF-NPs solution was purified by ultrafiltration (10 K, 4000 rpm) several times. The final concentration of DERF-NPs was determined by the concentration of SIR or BDP or CS.

**Preparation of DERF-NO.** For preparation of DERF-NO, a mixed tetrahydrofuran (THF) solution (2 mL) containing SIR-NO (100 μg), PSMA (0.5 mg), BSBT (100 μg), and Pluronic F127 (20 mg) was rapidly injected into distilled-deionized water (10 mL) under sonication. After sonication for another

10 min, the solution was evaporated at 50 °C by rotary evaporation to remove excess THF. Finally, the DERF-NO solution was purified by ultrafiltration (10 K, 4000 rpm) several times. The final concentration of DERF-NO was determined by the concentration of SIR-NO.

**NIR-II fluorescence imaging in solution.** Experiments to measure NIR-II fluorescence were performed in PBS (10 mM) buffer solutions. For fluorescence imaging, all NIR-II images were collected on a home-built small animal imaging system with 640 × 512 pixel 2D InGaAs NIRvana CCD camera under the same imaging window (1000-1700 nm) upon excitation at 660 nm (optical fiber output power density: 0.6 W/cm<sup>2</sup>, exposure time: 200 ms) and 808 nm (optical fiber output power density: 0.8 W/cm<sup>2</sup>, exposure time: 200 ms), respectively. And the imaging parameters were consistent for in vitro NIR-II fluorescence imaging unless otherwise stated. The fluorescence intensity in each image was quantified by applying a region of interest (ROI) over the image, with the LightField imaging software and ImageJ.

**Tissue-penetration studies.** For imaging under chicken tissues, DERF-NP4 (50 µg/mL SIR, 50 µg/mL BSBT) solutions were placed under chicken tissues of varying thickness (0, 0.1, 0.2, 0.4 and 0.6 cm). For imaging under Intralipid, DERF-NP4 (50 µg/mL SIR, 50 µg/mL BSBT) solutions were placed under Intralipid of varying thickness (0, 0.1, 0.2, 0.3 and 0.4 cm). Then the NIR-II fluorescent images were acquired for 200 ms at 1000-1700 nm upon excitation at 660 nm and 808 nm, respectively.

**Cell culture.** 4T1 Cells were cultured in high glucose Dulbecco's Modified Eagle Medium (DMEM, Hyclone) supplemented with 10% fetal bovine serum

(FBS, BI), and 1% antibiotics (100 U/mL penicillin and 100 µg/mL streptomycin, Hyclone) at 37 °C and 5% CO<sub>2</sub>. Cells were carefully harvested and split when they reached 80% confluence to maintain exponential growth.

***In vivo* experiment.** All animal procedures were performed in accordance with the Guidelines for the Care and Use of Laboratory Animals of Hunan University, and experiments were approved by the Animal Ethics Committee of the College of Biology (Hunan University). All NIR-II images were collected on a home-built small animal imaging system with 640 × 512 pixel 2D InGaAs NIRvana CCD camera. Images were processed with the LightField imaging software and ImageJ.

**Lymphmatic inflammation.** To establish the lymphmatic inflammation, mice were intradermally (i.d.) injected with 50 µL (2.0 mg/mL) lipopolysaccharide or 50 µL saline into the rear paw, and followed 4 h later by an additional i.d. injection of 50 µL DERF-NO (200 µg/mL SIR, 200 µg/mL BSBT, pH 5.0 buffer solution), and thereafter imaged by an NIR-II fluorescence imaging system. Before imaging, the mice were anaesthetized using rodent ventilator with 2 L/min air mixed with 4% isoflurane. Images were recorded at different time post-injection to visualize the dynamic drainage and get images ( $\lambda_{\text{ex}} = 660 \text{ nm}$  and 808 nm,  $\lambda_{\text{em}} = 1000 - 1700 \text{ nm}$ , exposure time was set to 500 ms).

***In vivo* tumor imaging of macrophage polarization.** Mice bearing 4T1 xenograft tumor were i.t.-injected with 25 µL of PBS or 20 µg/mL of IFN- $\gamma$  then i.v.-injected with 200 µL DERF-NO (200 µg/mL SIR-NO, 200 µg/mL BSBT). Then, mice were imaged by fluorescence imaging mode. For isolation of tumor cells and flow cytometric analysis, 24 hours post-i.t. injection of IFN- $\gamma$ ,

representative tumors from each group were harvested, minced and treated with 1 mg/ml type I collagenase and 0.1 mg/ml of DNase I, followed by incubation for 1 h at 37 °C and 5% CO<sub>2</sub>. The cell suspension was passed through a 70 µm filter to remove debris and to obtain a single cell suspension. Then, the tumor cells were preincubated (30 min, 4 °C) with anti-CD16/32 monoclonal antibody (0.5 µg, Fc block, clone 2.4G, BD Biosciences) to block nonspecific binding and then stained (30 min, 4 °C) with appropriate dilutions of various combinations of the following fluorochrome-conjugated antibodies: anti-F4/80-PE-Cy5 (0.25 µg, clone BM8), and anti-CD80-APC (0.06 µg, clone 16-10A1). Post-staining, the samples were washed twice to remove unbound antibodies and analyzed using flow cytometry.

***In vivo* imaging of lymphatic metastasis.** The establishment of lymphatic metastasis model in mice was carried out by inoculation with 4T1 tumor cells on the right flank of BALB/c mice. The mice were raised for three weeks to produce lymphatic metastasis in mice. Mice were injected by an additional i.d. injection of 50 µL DERF-NO (200 µg/mL SIR-NO, 200 µg/mL BSBT, pH 5.0 buffer solution) in the hind paws. After administration, mice were anaesthetized using rodent ventilator with 2 L/min air mixed with 4% isoflurane. The NIR-II images were collected on a small animal imaging system with 640 × 512 pixel 2D InGaAs NIRvana CCD camera. The signal intensity of lymph nodes at the tumor site and normal site were integrated and calculated, respectively. The signal ratio of tumor site to normal site (T/N ratio) was applied to assess the metastasis of the cancer cell. ( $\lambda_{ex}$  = 660 nm and 808 nm,  $\lambda_{em}$  = 1000 – 1700 nm, exposure time was set to 500 ms).

**Table S1.** The summary of ratiometric NIR-II NO probes.

<b>Probe</b>	<b><math>\lambda_{ex}/</math> nm</b>	<b><math>\lambda_{em}/</math> nm</b>	<b>Imaging channel</b>	<b>Imaging mode</b>	<b>Detection limit</b>	<b>Refere nce</b>
RAPNP	808	940/ 1120	860-940 nm/ 1100-1200 nm	single-excitation and dual-emission	0.26 $\mu$ M	5
DCNP@M	808/	1050/	1050 nm/	dual-excitation	0.61 $\mu$ M	6
PS@IR	980	1550	1550 nm	and dual-emission		
RP-NH <sub>2</sub> - 1.5 NPs	635/ 808	1000/ 1550	1000-1400 nm/ 1500-1700 nm	dual-excitation and dual-emission	0.30 $\mu$ M	7
DERF-NO	660/ 808	1028	1000-1700 nm	dual-excitation and single-emission	45.8 nM	This work

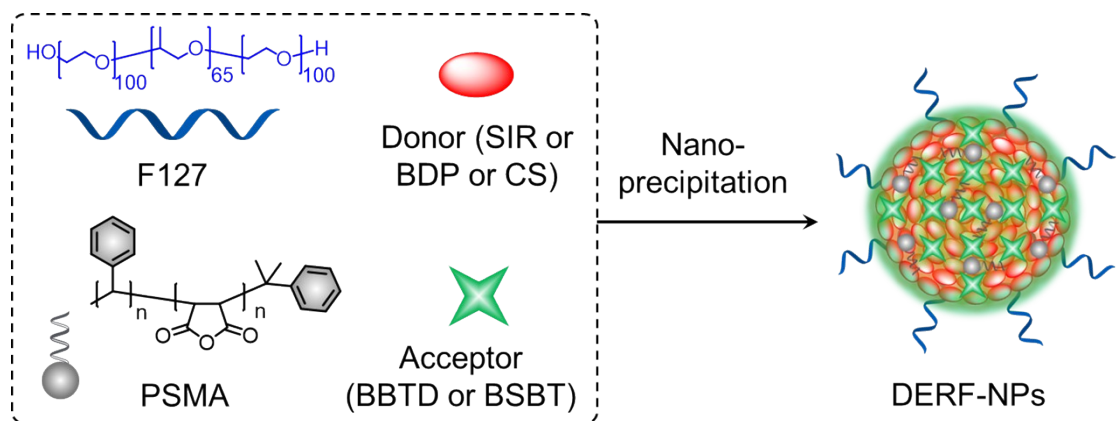


**Fig. S1** Schematic illustration for preparation of DERF-NPs.

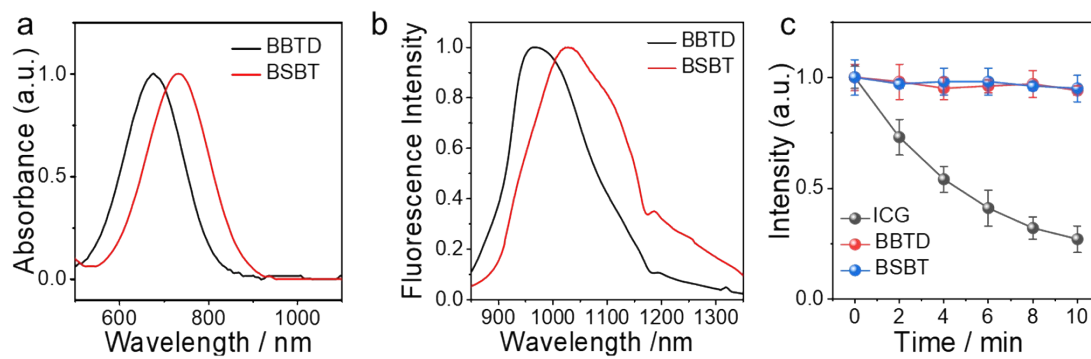


**Fig. S2** (a) Absorption spectra and (b) fluorescence emission spectra of BBTD and BSBT. Excitation wavelength: 808 nm. (c) Normalized fluorescence intensity of ICG, BBTD, and BSBT nanoparticles in PBS buffer solution upon constant 808 nm laser ( $100 \text{ mW/cm}^2$ ) beam exposure for different times.

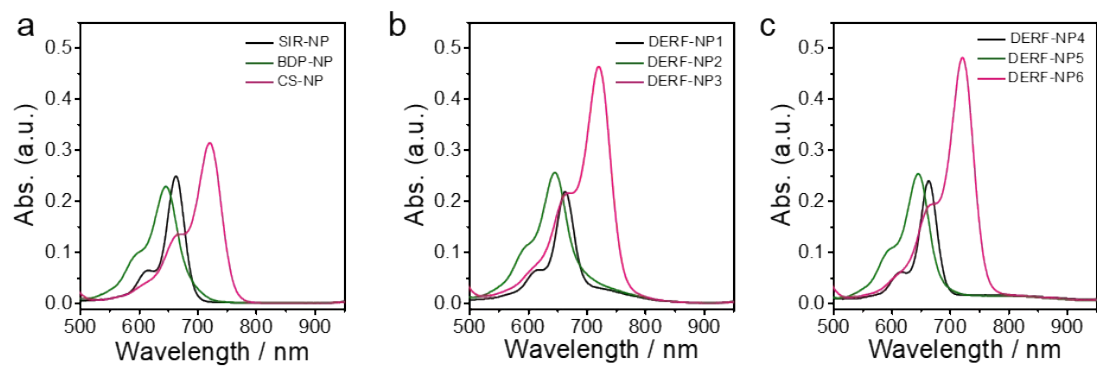


**Fig. S3** (a) Normalized absorption spectra of SIR-NP, BDP-NP and CS-NP. (b) Normalized absorption spectra of DERF-NP1-3. (c) Normalized absorption spectra of DERF-NP4-6.

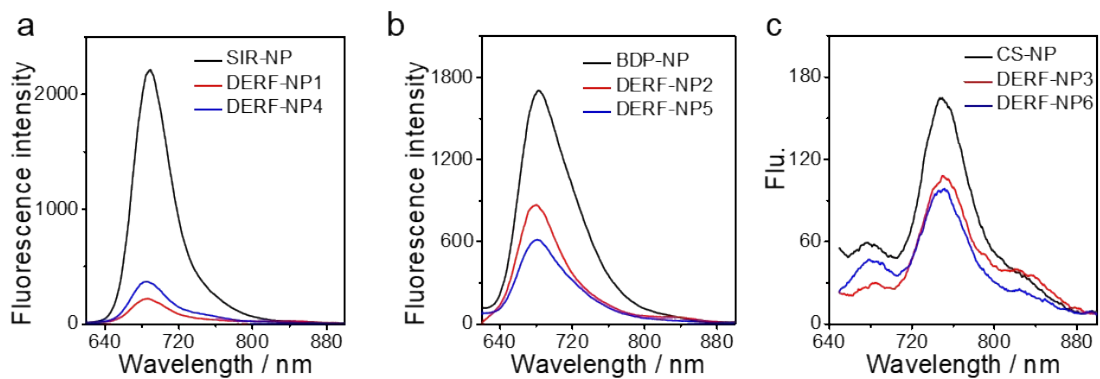


**Fig. S4** (a) Normalized fluorescence emission spectra of SIR-NP, DERF-NP1 and DERF-NP4. (b) Normalized fluorescence emission spectra of BDP-NP, DERF-NP2 and DERF-NP5. (c) Normalized fluorescence emission spectra of CS-NP, DERF-NP3 and DERF-NP6. Excitation wavelength: 600 nm.

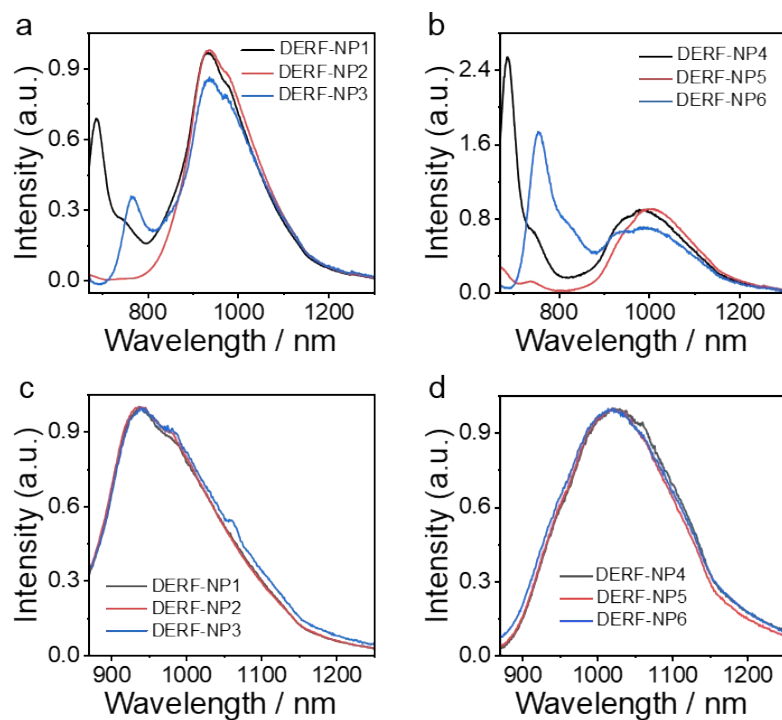


**Fig. S5** Normalized NIR-II fluorescence emission spectra of (a) DERF-NP1~3 and (b) DERF-NP4~6 upon excitation at 660 nm. Normalized NIR-II fluorescence emission spectra of (c) DERF-NP1~3 and (d) DERF-NP4~6 upon excitation at 808 nm.

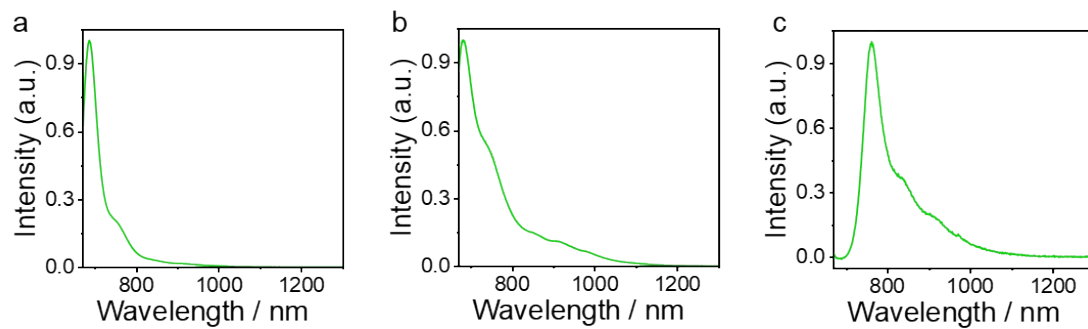


**Fig. S6** Normalized NIR-II fluorescence emission spectra of (a) SIR-NP, (b) BDP-NP and (c) CS-NP. Excitation wavelength: 660 nm.

**Table S2.** The summary of photophysical properties for BBTD, BSBT, SIR, BDP, CS.  $\lambda_{\text{abs}}/\text{nm}$ : The maximal absorption.  $\lambda_{\text{em}}/\text{nm}$ : The maximal emission.  $\epsilon$ : molar extinction coefficient.  $\Phi_f$ : Quantum yields.

<sup>a</sup> Relative fluorescence quantum yield ( $\Phi_f$ ) in toluene was measured relative to ICG (13% in DMSO).

<sup>b</sup> Relative fluorescence quantum yield ( $\Phi_f$ ) in EtOH containing 0.1 mM HCl was measured relative to ICG (13% in DMSO).

<sup>c</sup> Relative fluorescence quantum yield ( $\Phi_f$ ) in dichloromethane was measured relative to ICG (13% in DMSO).

<sup>d</sup> Relative fluorescence quantum yield ( $\Phi_f$ ) in EtOH was measured relative to ICG (13% in DMSO).

A/D	$\lambda_{\text{abs}}/\text{nm}$	$\lambda_{\text{em}}/\text{nm}$	Stokes shift	$\epsilon$ ( $\times 10^4 \text{ M}^{-1} \text{ cm}^{-1}$ )	$\Phi_f$ (%)
BBTD	700	967	267	1.08	3.8 <sup>a</sup>
BSBT	756	1028	272	0.95	1.6 <sup>a</sup>
SIR	653	672	19	11.8	34 <sup>b</sup>
BDP	641	661	20	10.3	45 <sup>c</sup>
CS	702	733	31	13.9	39 <sup>d</sup>

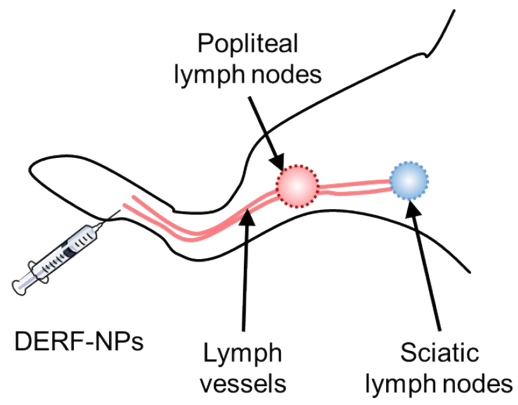


**Fig. S7** In vivo NIR-II fluorescence images and corresponding ratiometric images of mouse lymphatic drainage at different times postinjection of DERF-NP4.

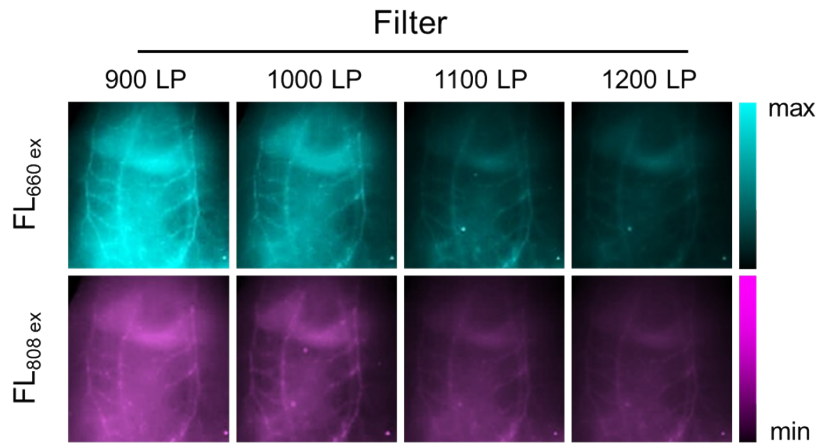
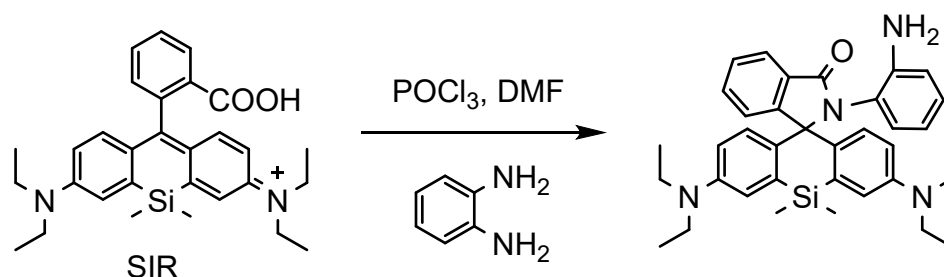
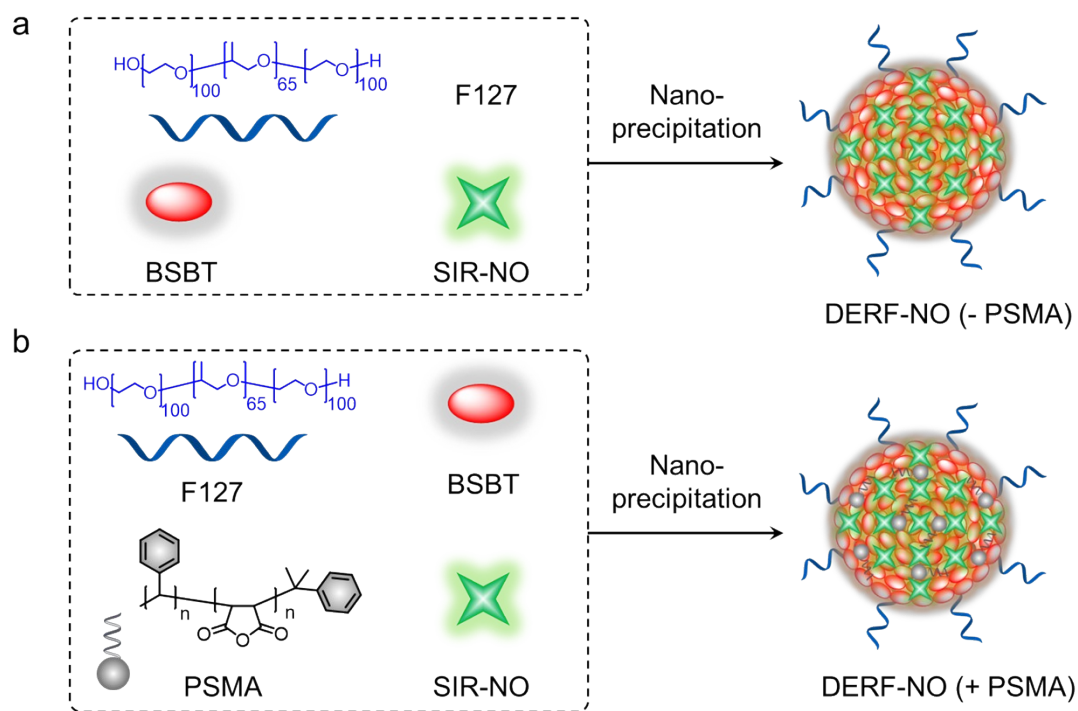


**Fig. S8** Representative fluorescent images of abdominal blood vessels of mice after i.v. injection of DERF-NP4 under different emission filters upon excitation at 660 nm and 808 nm. Exposure time: 200 ms (900 nm LP), 500 ms (1000 nm LP), 1000 ms (1100 nm LP), 2000 ms (1200 nm LP).

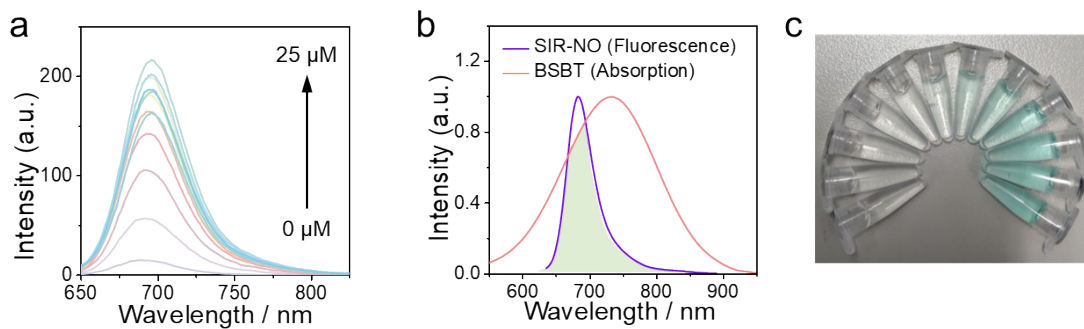


**Scheme S3.** The synthetic route of SIR-NO.

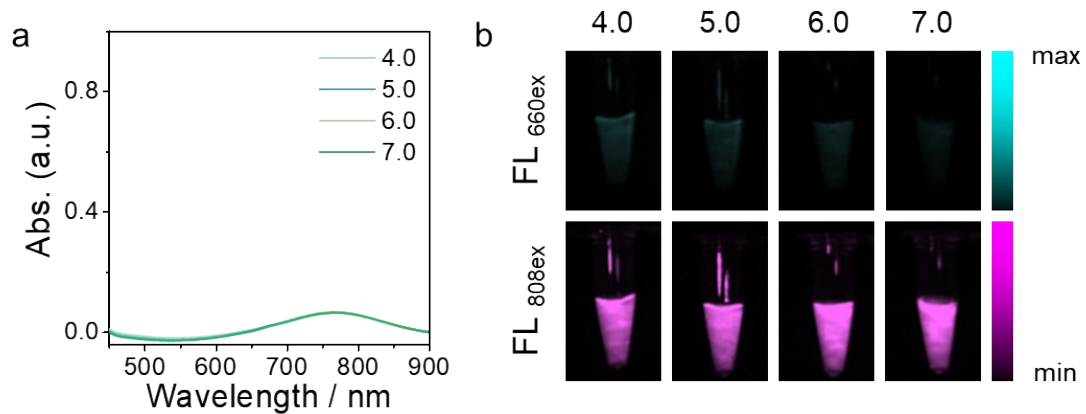
**Synthesis of SIR-NO.** To a solution of compound SIR (484 mg, 1.0 mmol) in dry 1, 2-dichloroethane (5.0 mL) at room temperature, phosphorus oxychloride (460 mg, 3.0 mmol) was added dropwise over a period of 5 minutes. After being refluxed for 4 hours, the reaction mixture was cooled and concentrated under vacuum to give a blue solid. This blue solid was dissolved in dry acetonitrile (5.0 mL). The blue solution was slowly added to a solution of *o*-diaminobenzene (540 mg, 5.0 mmol) in dry acetonitrile (5.0 mL) containing triethylamine (5.0 mL). After stirring at room temperature overnight, the mixture was concentrated in vacuo and the crude product was purified by column chromatography on silica gel (ethyl acetate: petroleum ether=1:4) to give SIR-NO as a white solid (327 mg, 57% yield). <sup>1</sup>H NMR (300 MHz, CDCl<sub>3</sub>): δ = 8.06 (1 H, d, J=6.8), 7.60-7.50 (2 H, m), 7.22 (1 H, d, J=6.4), 6.93 (1 H, t, J=7.6), 6.72 (4 H, d, J=6.9), 6.55 (3 H, dd, J=16.2, 8.5), 6.37 (1 H, t, J=7.5), 5.85 (1 H, d, J=7.9), 3.43-3.32 (8 H, m), 3.20 (1 H, s, J=6.6), 1.18 (12 H, t, J=6.9), 0.44 (3 H, s), -0.31 (3 H, s). <sup>13</sup>C NMR (75 MHz, CDCl<sub>3</sub>): δ = 167.3, 155.1, 146.1, 145.5, 137.2, 132.6, 132.4, 131.3, 130.6, 130.2, 128.8, 127.8, 124.3, 123.4, 122.1, 118.0, 116.6, 114.8, 113.9, 75.1, 44.2, 12.5, -0.6, -1.7.



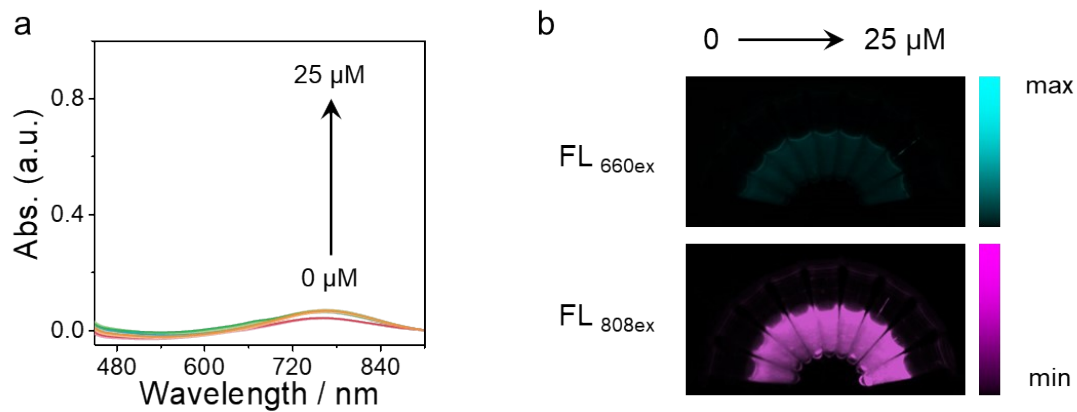
**Fig. S9** Schematic illustration for preparation of (a) DERF-NO (-PSMA) and (b) DERF-NO (+PSMA).



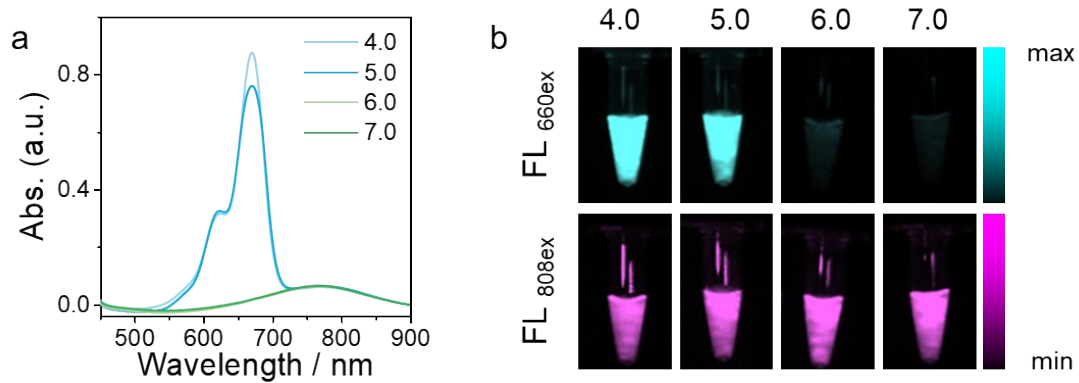
**Fig. S10** (a) Fluorescent emission spectra of SIR-NO treated with different concentrations of NO in the NIR-I region. (b) Spectra overlap shows the absorption spectra of BSBT and fluorescence spectra of SIR-NO after incubation with NO. (c) Photograph of SIR-NO treated with different concentrations of NO.



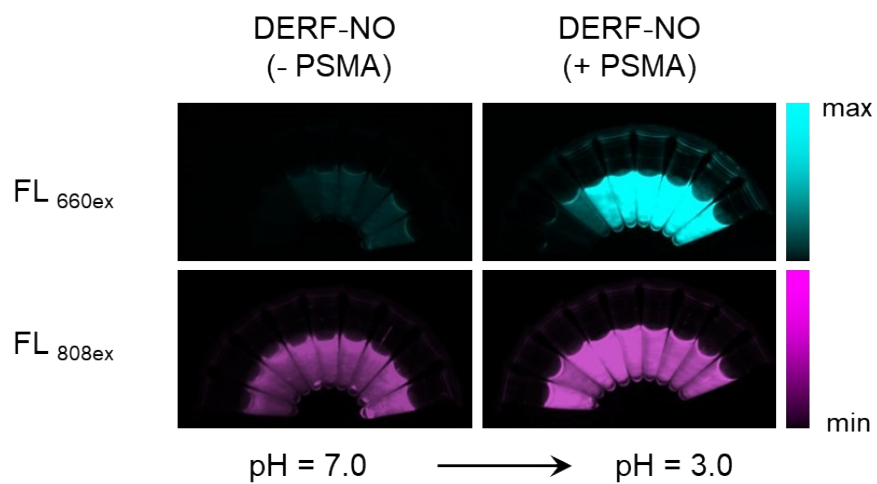
**Fig. S11** (a) Absorption spectra of DERF-NO (-PSMA) in different pH buffer solution. (b) Representative fluorescent images upon excitation at 660 nm and 808 nm of DERF-NO (-PSMA) in different pH buffer solution.



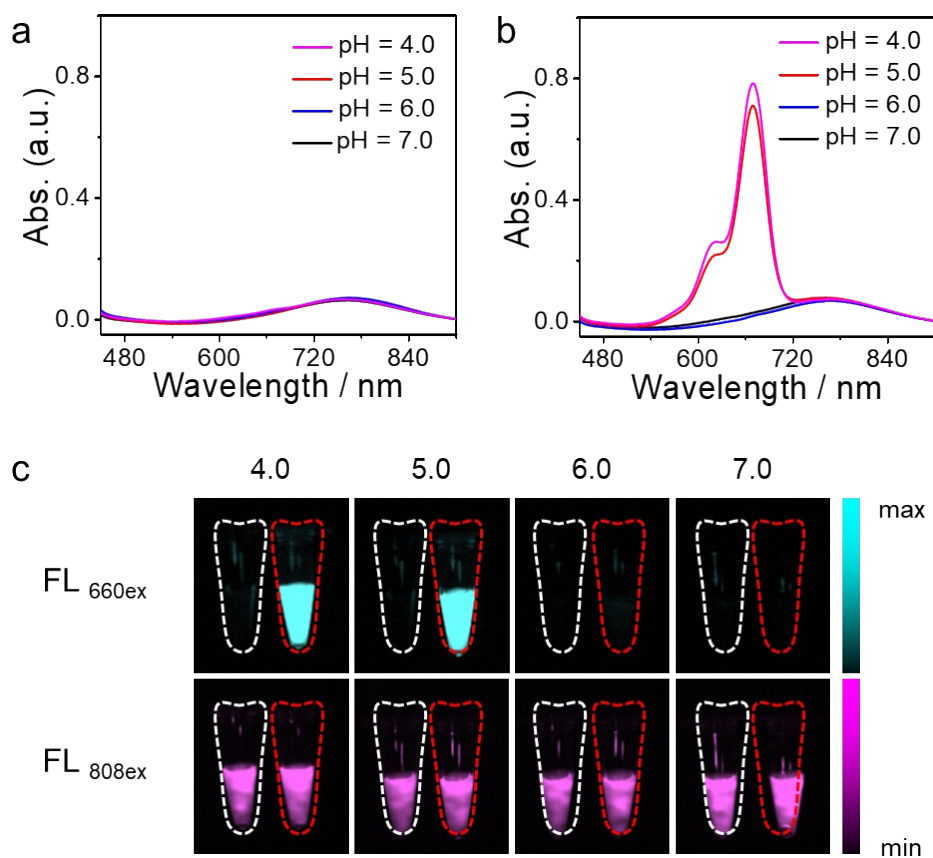
**Fig. S12** (a) Absorption spectra of DERF-NO (-PSMA) treated with different concentrations of NO in pH 7.4 PBS buffer solution. (b) Representative NIR-II fluorescent images of DERF-NO (-PSMA) treated with different concentrations of NO in pH 7.4 PBS buffer solution upon excitation at 660 nm and 808 nm.



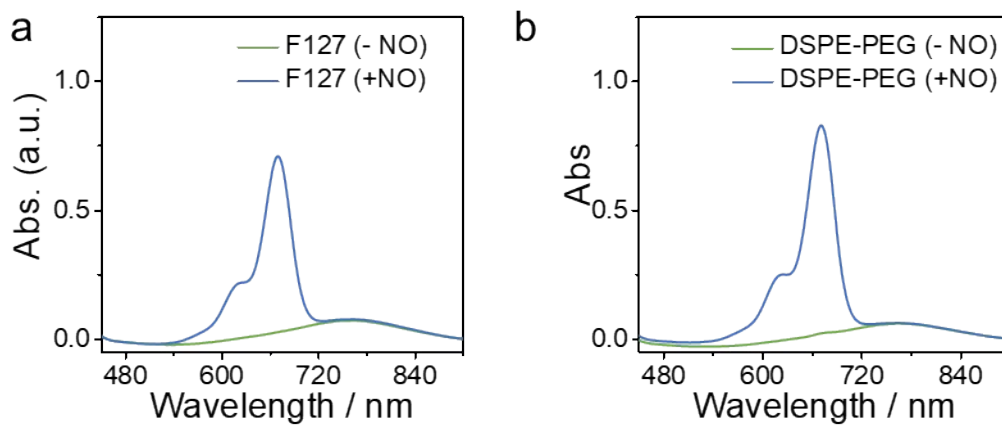
**Fig. S13** (a) Absorption spectra of DERF-NO (-PSMA) in NO (25 μM) pre-treated solution with different pH values. (b) Representative fluorescent images upon excitation at 660 nm and 808 nm of DERF-NO (-PSMA) treated with NO (25 μM) in different pH buffer solution.



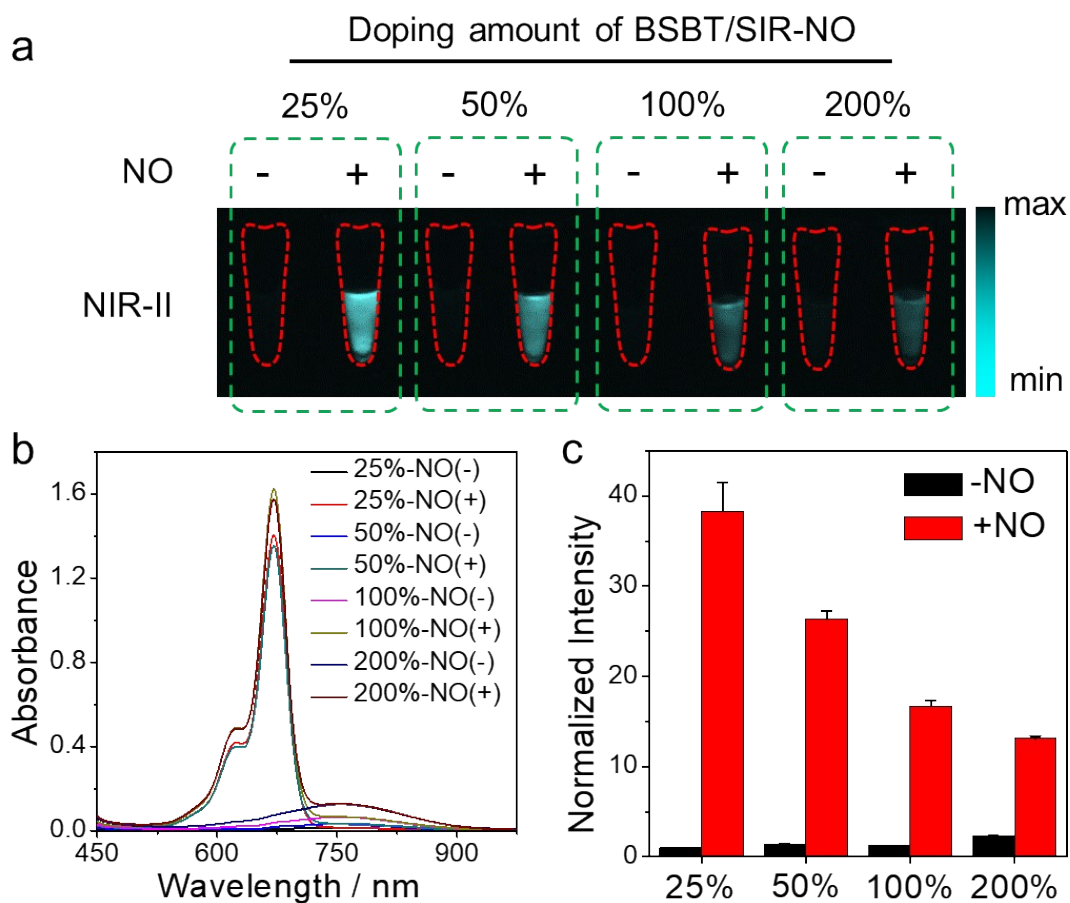
**Fig. S14** Representative fluorescent images upon excitation at 660 nm and 808 nm of DERF-NO (-PSMA) and DERF-NO (+PSMA) treated with NO (25  $\mu$ M) in different pH buffer solution.



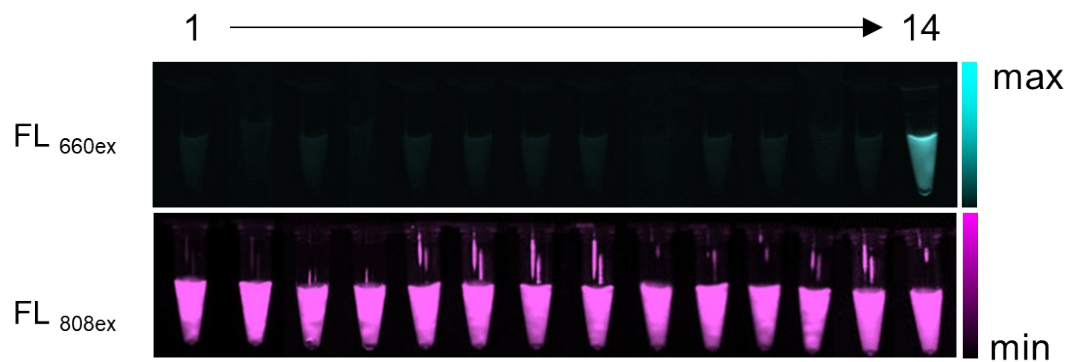
**Fig. S15** (a) Absorption spectra of DERF-NO (+PS) in different pH buffer solution without NO incubation. (b) Absorption spectra of DERF-NO (+PS) in NO (25  $\mu$ M) pre-treated solution with different pH values. (c) Representative fluorescent images upon excitation at 660 nm and 808 nm of DERF-NO (+PS) treated with (red dotted box) and without (white dotted box) NO (25  $\mu$ M) in different pH buffer solution.



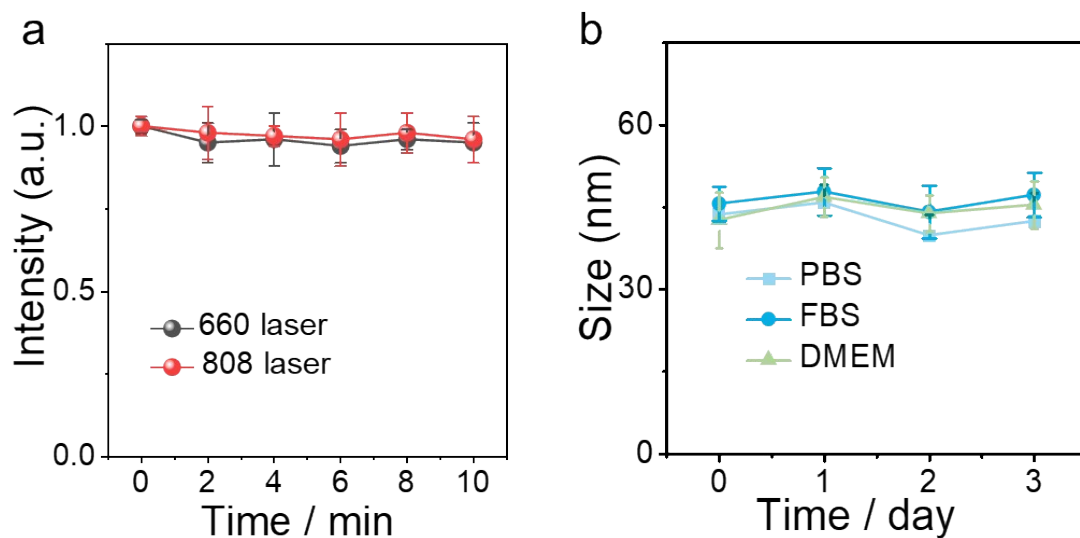
**Fig. S16** (a) Absorption spectra of F127-doped DERF-NO before and after incubation with NO (25  $\mu\text{M}$ ) in pH 5.5 buffer solution. (b) Absorption spectra of DSPE-PEG-doped DERF-NO before and after incubation with NO (25  $\mu\text{M}$ ) in pH 5.5 buffer solution.



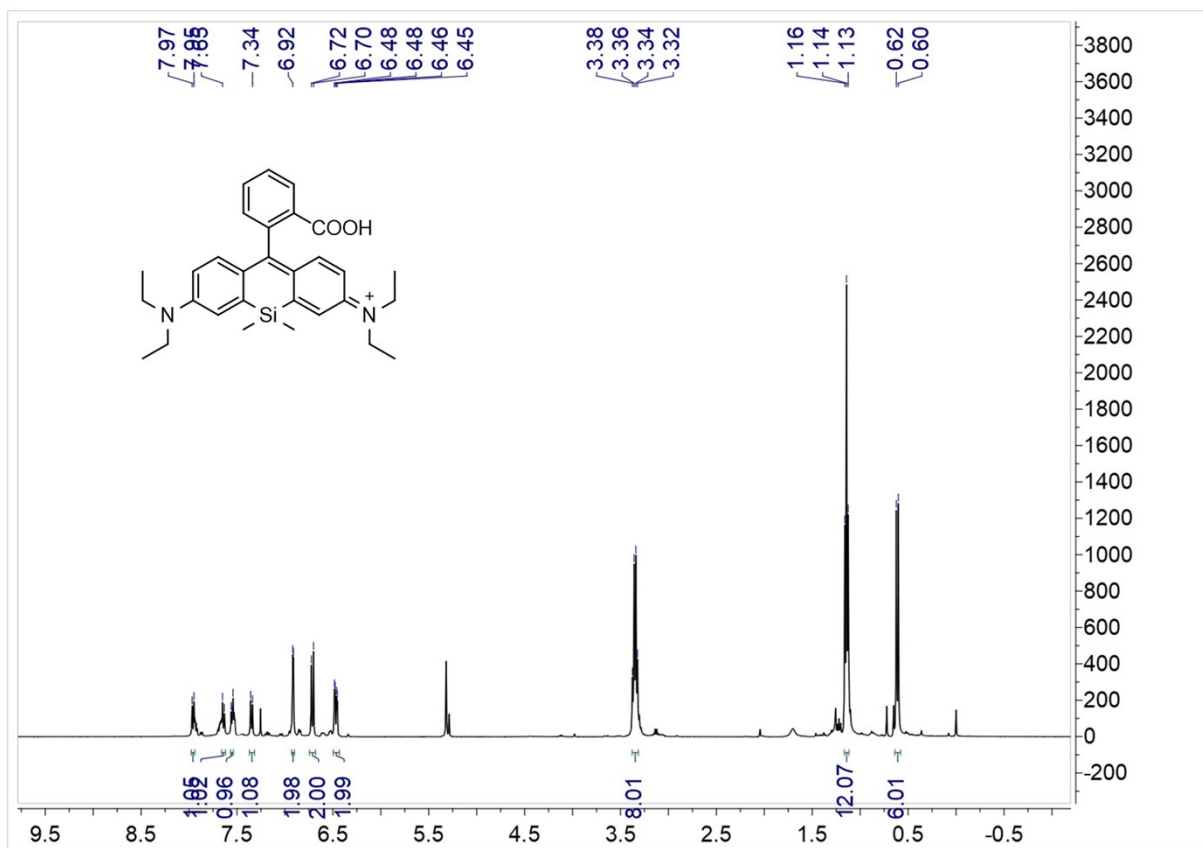
**Fig. S17** (a) Representative NIR-II fluorescent images (b) absorption spectra and (c) normalized fluorescent intensity of DERF-NO with different doping amounts of BSBT/SIR-NO after incubation with NO (25  $\mu$ M) in pH 5.5 buffer solution.

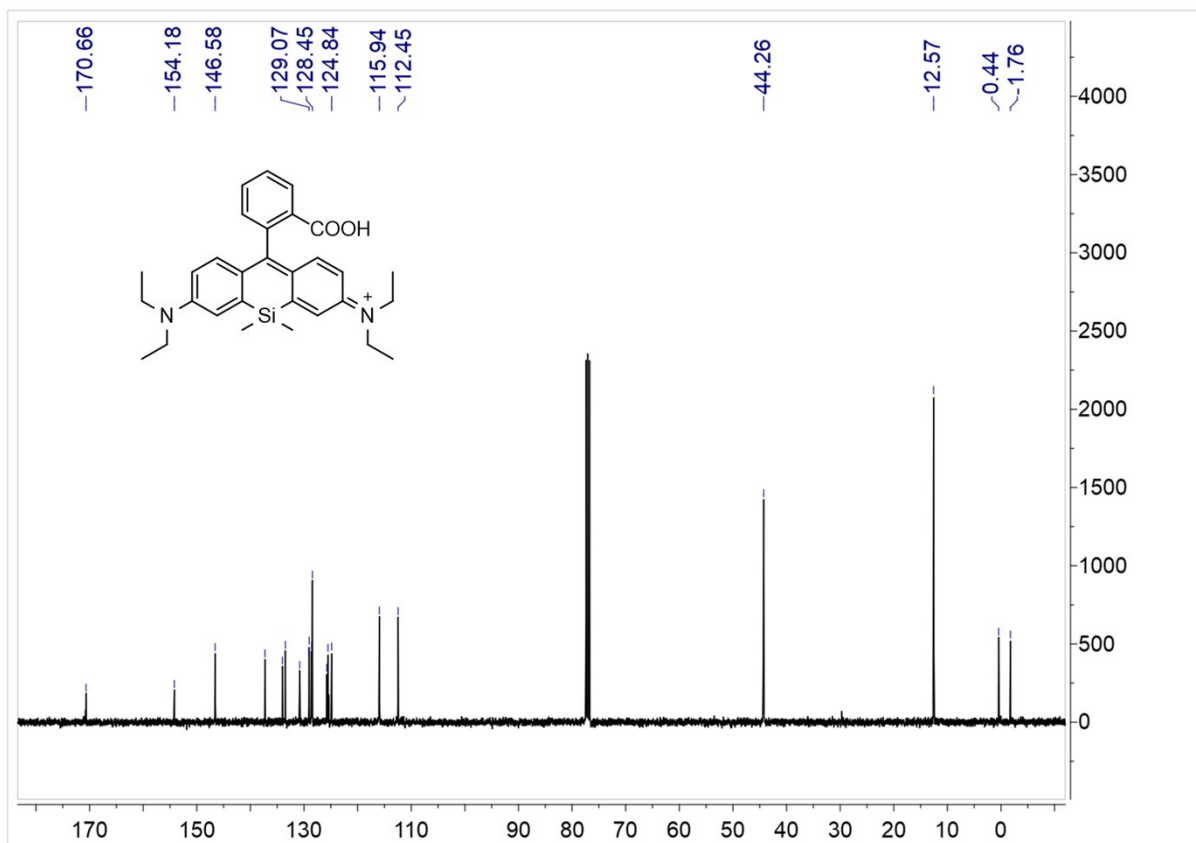


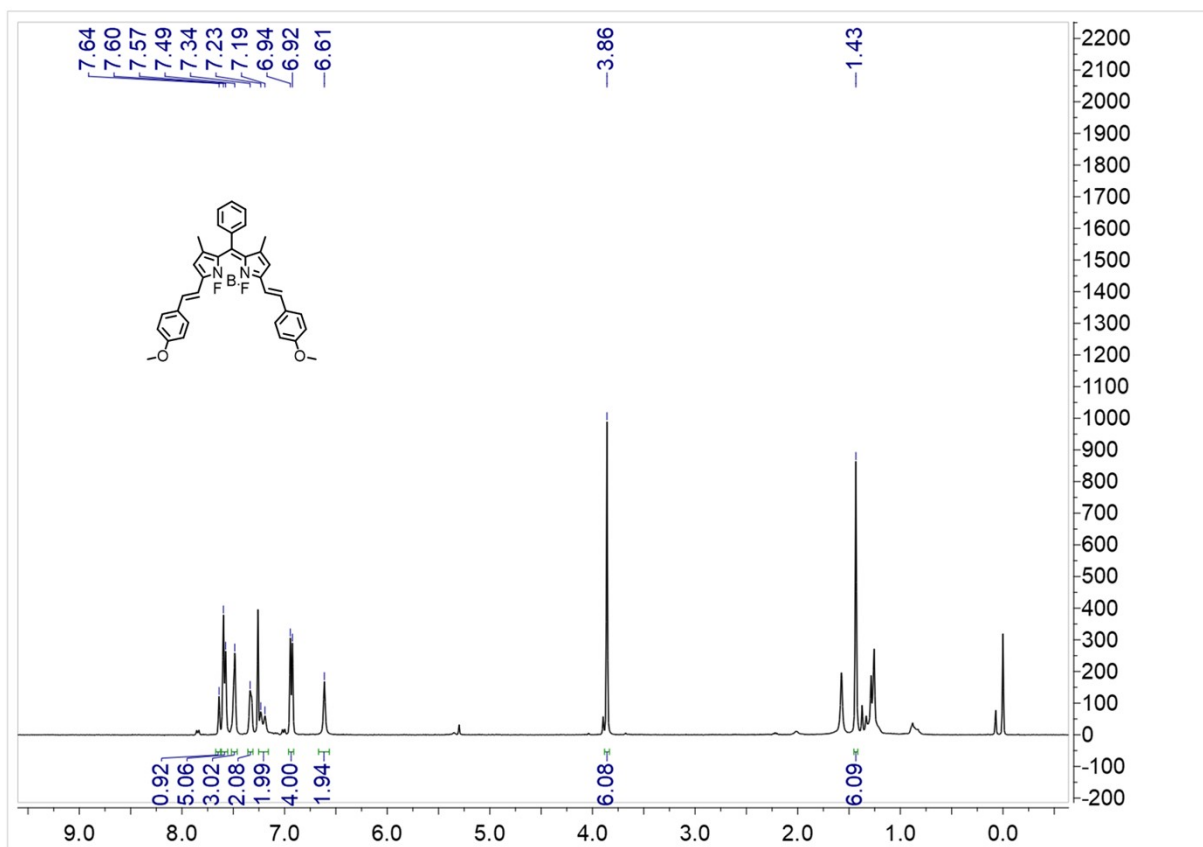
**Fig. S18** Representative NIR-II fluorescent of DERF-NO upon incubation with different interference species. 1. Blank, 2.  $\text{Na}^+$  (10 mM), 3.  $\text{K}^+$  (10 mM), 4.  $\text{Ca}^{2+}$  (10 mM), 5.  $\text{Fe}^{2+}$  (1 mM), 6.  $\text{H}_2\text{O}_2$  (250  $\mu\text{M}$ ), 7.  $\text{HClO}$  (50  $\mu\text{M}$ ), 8.  $\text{ONOO}^-$  (50  $\mu\text{M}$ ), 9.  $\text{O}_2^-$  (100  $\mu\text{M}$ ), 10.  $\text{t-BuOOH}$  (100  $\mu\text{M}$ ), 11.  $\cdot\text{OH}$  (100  $\mu\text{M}$ ), 12. Cys (500  $\mu\text{M}$ ), 13. GSH (1 mM), 14. NO (25  $\mu\text{M}$ ).

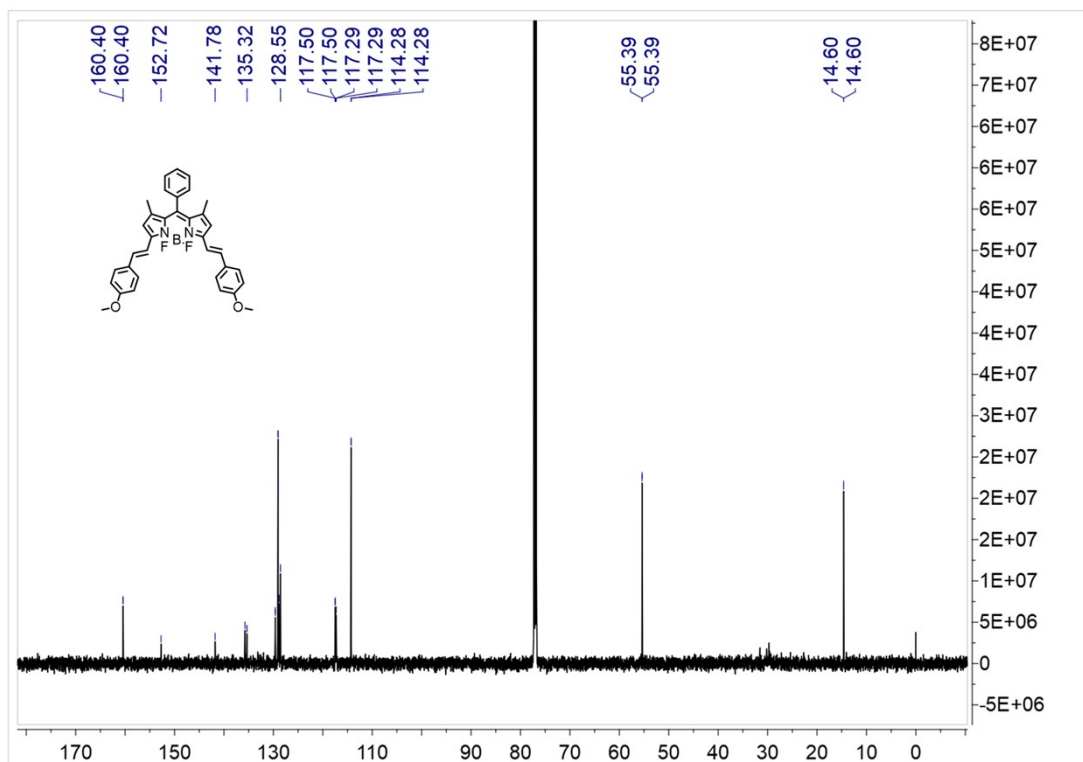


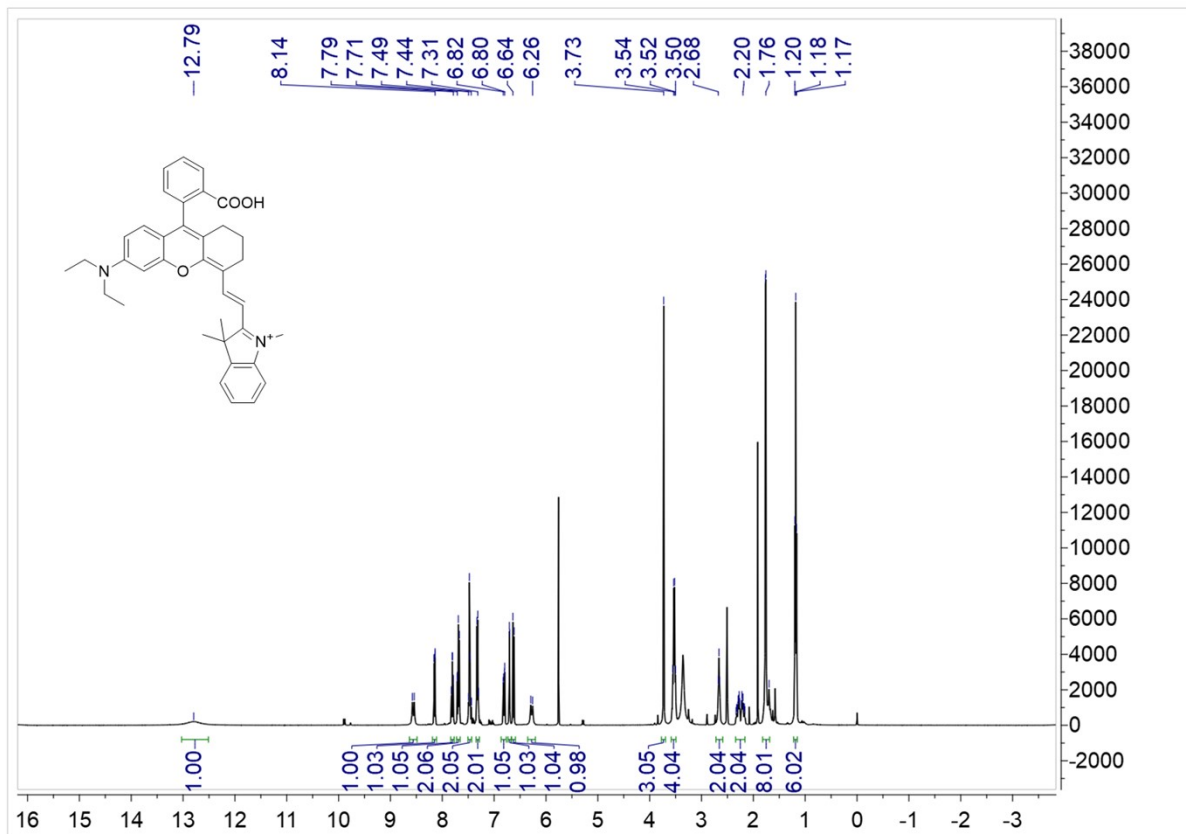
**Fig. S19** (a) Normalized fluorescence intensity of DERF-NO after incubation with NO in PBS buffer solution upon 660 and 808 nm laser ( $100 \text{ mW/cm}^2$ ) beam exposure for different times. (b) Hydrodynamic size of DERF-NO in PBS, FBS, DMEM as measured by dynamic light scattering (DLS).

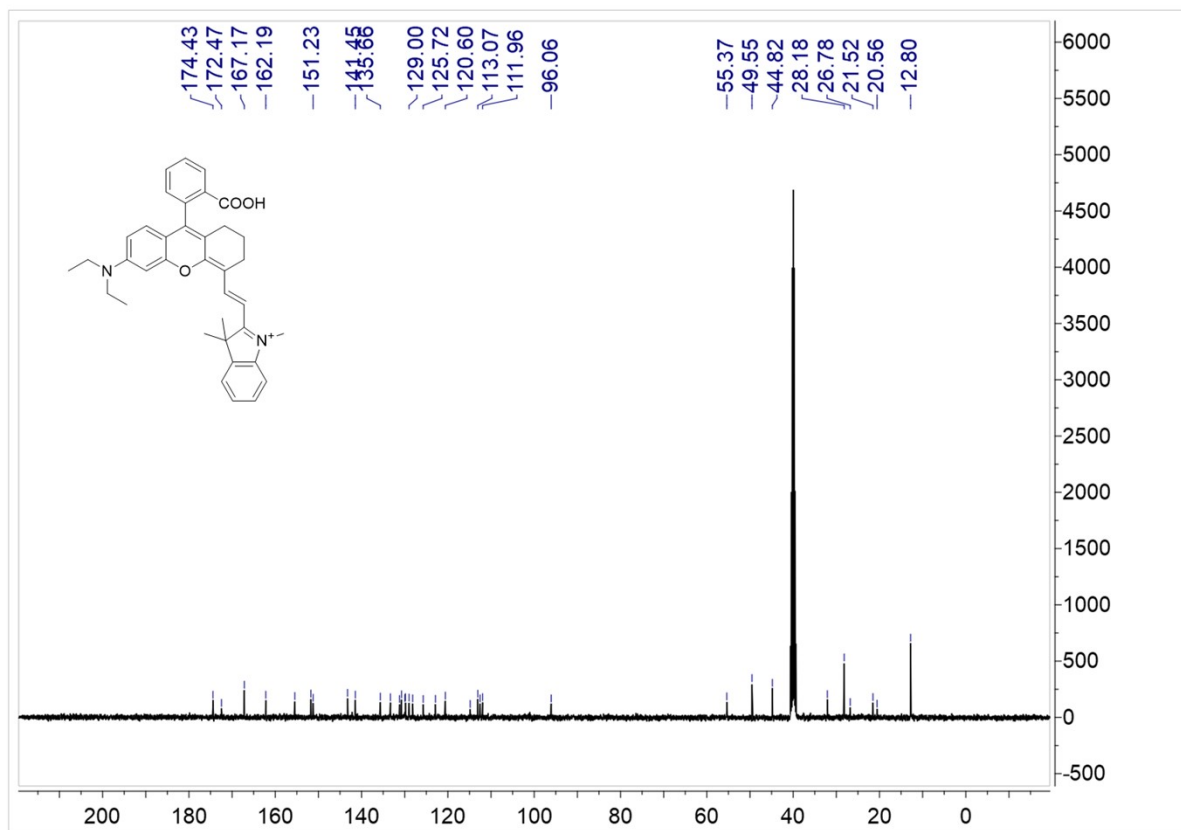


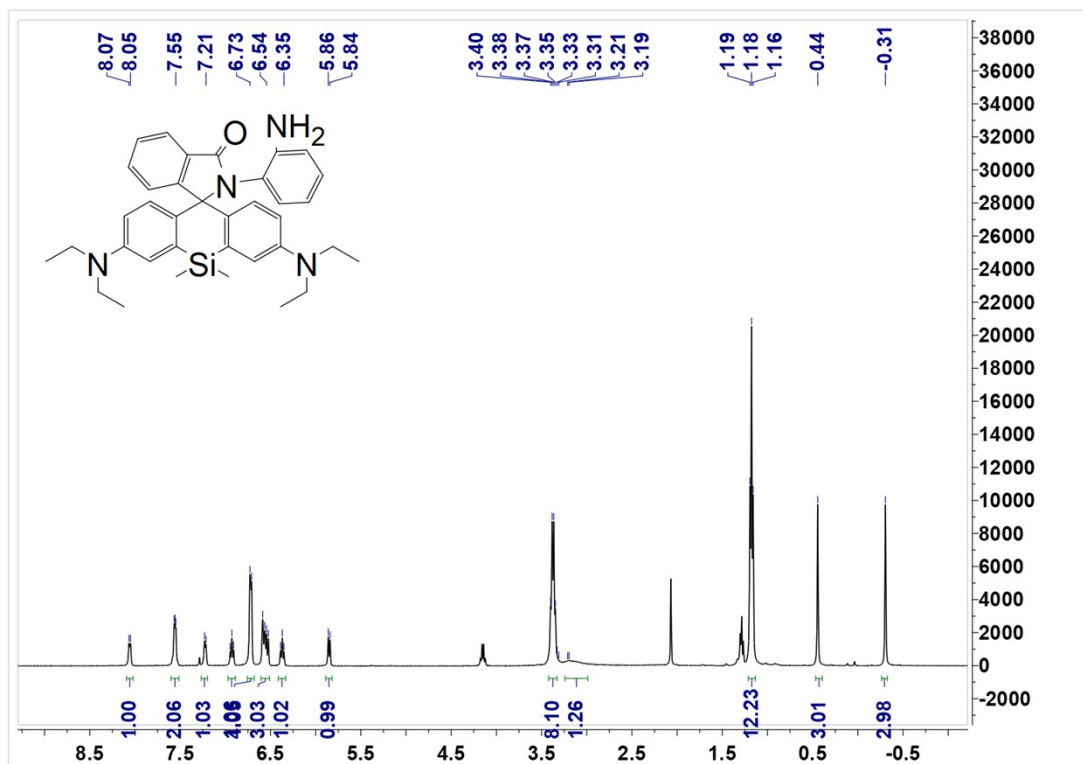


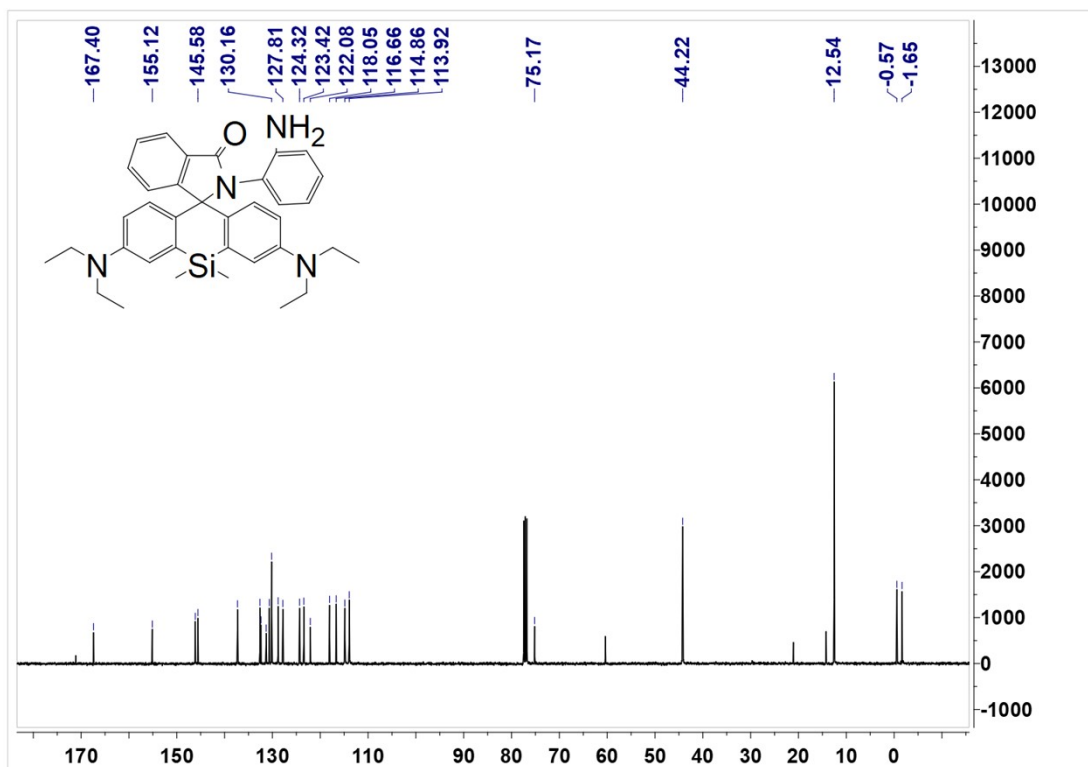


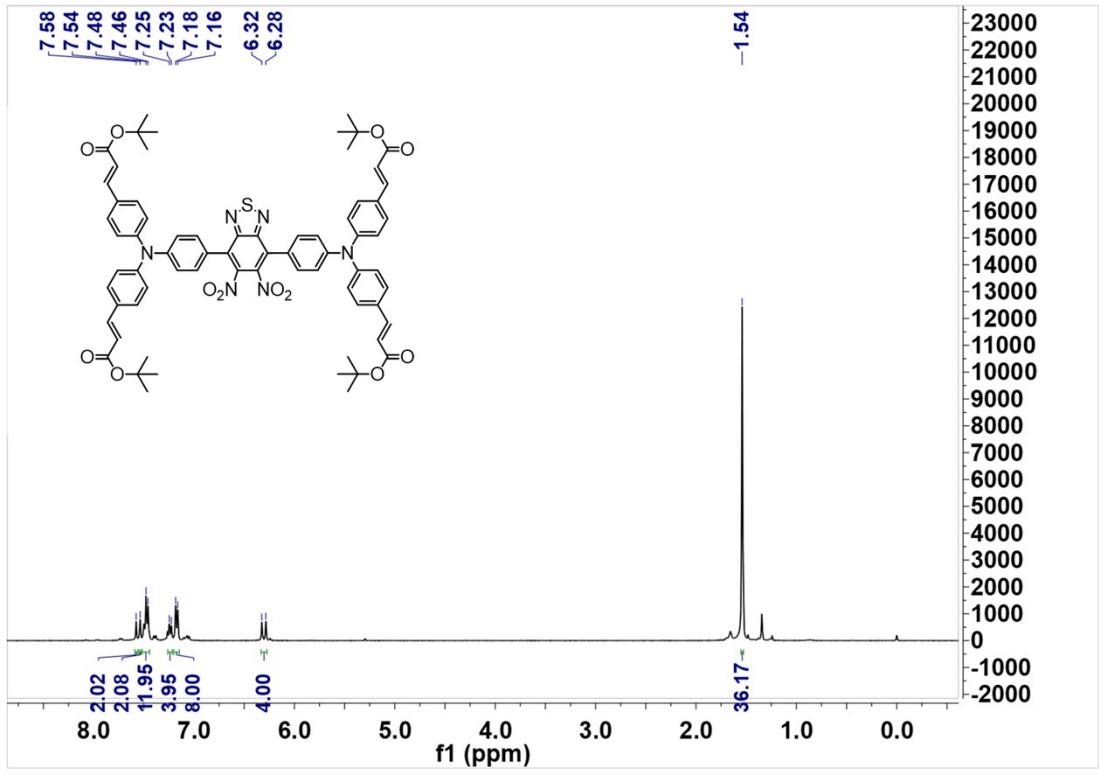


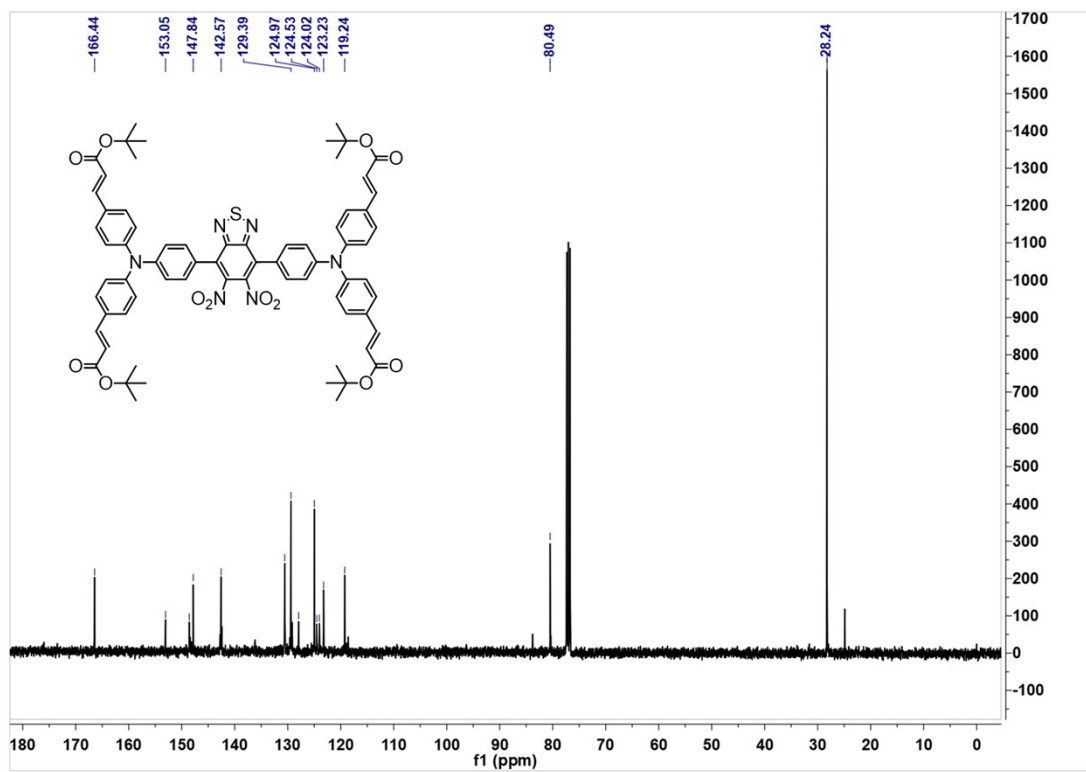


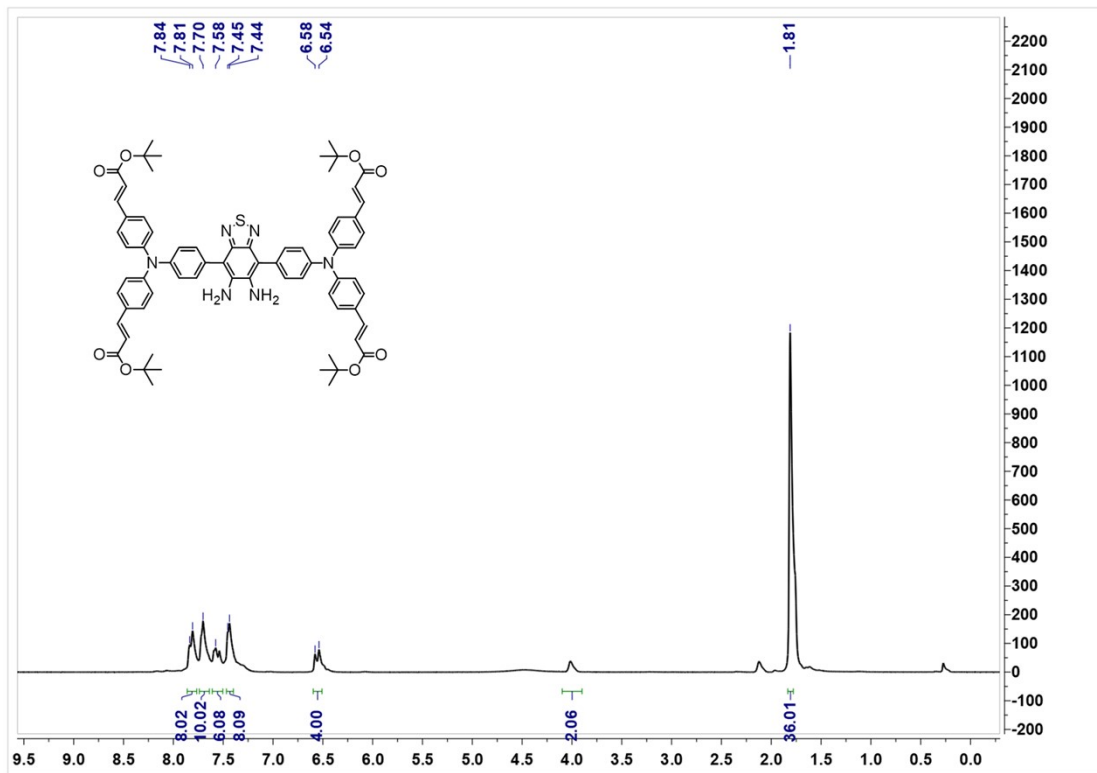


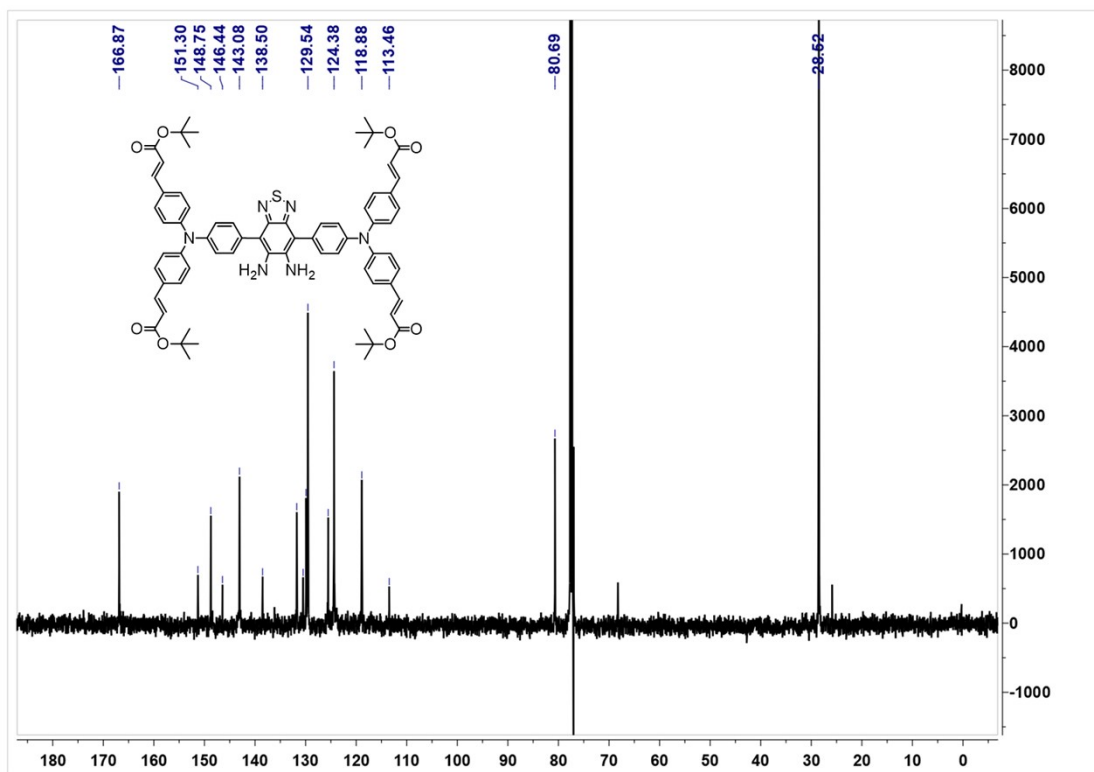


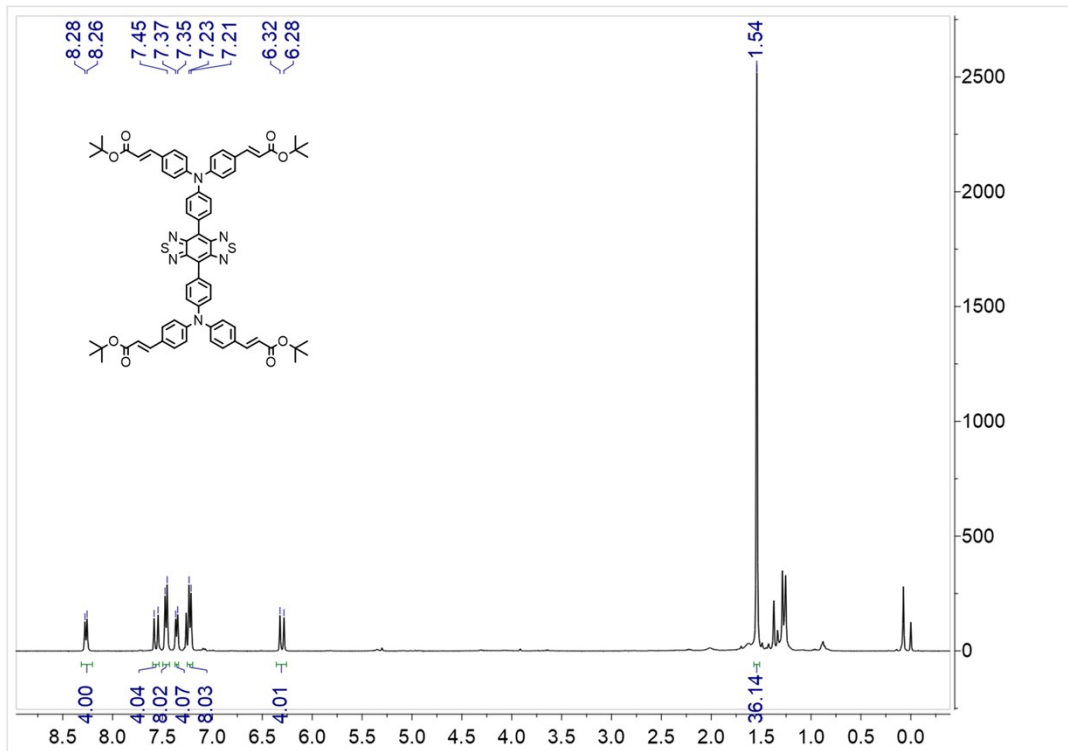


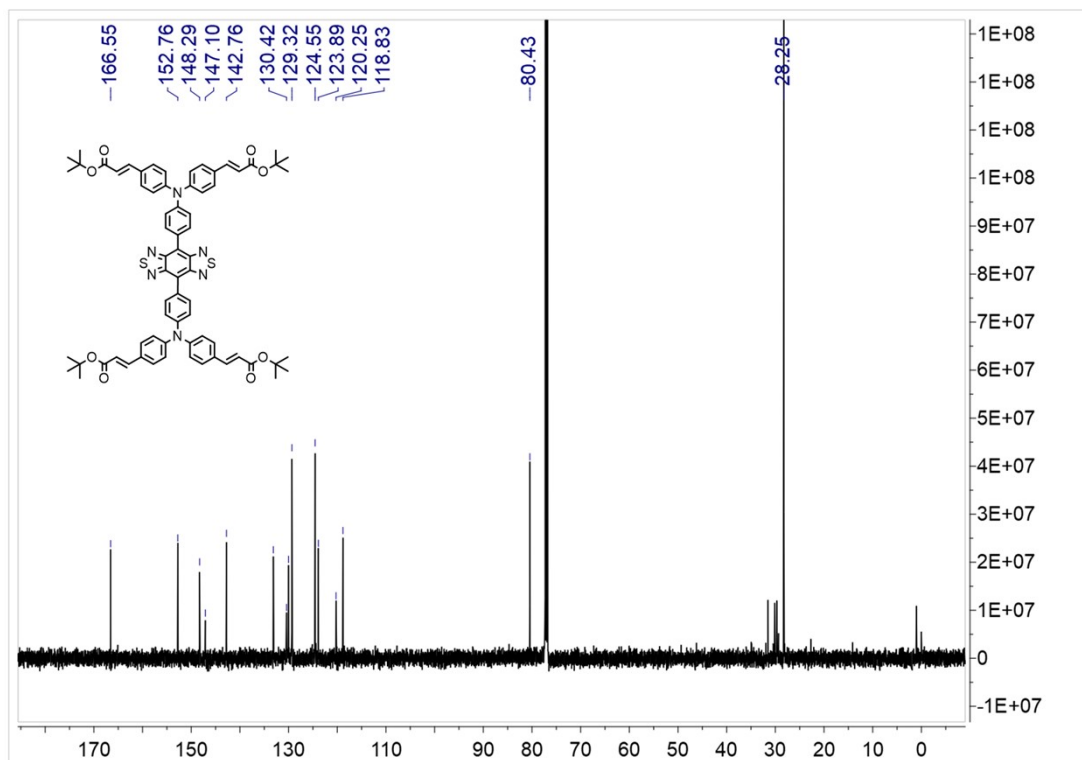


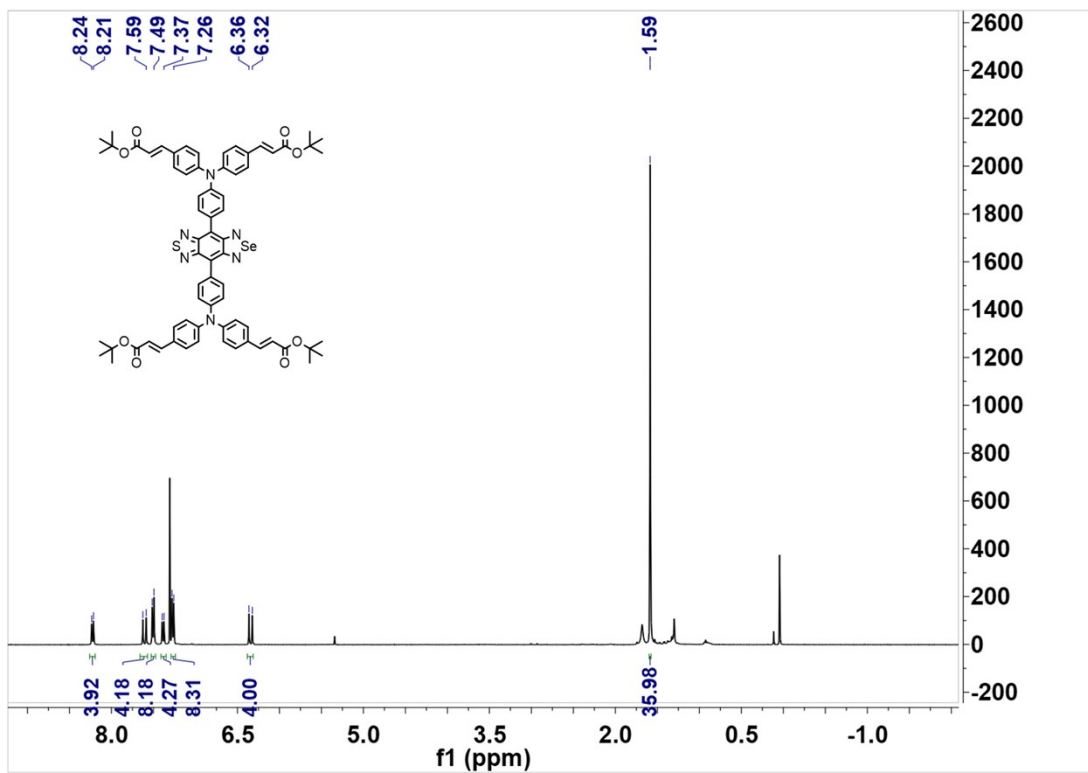


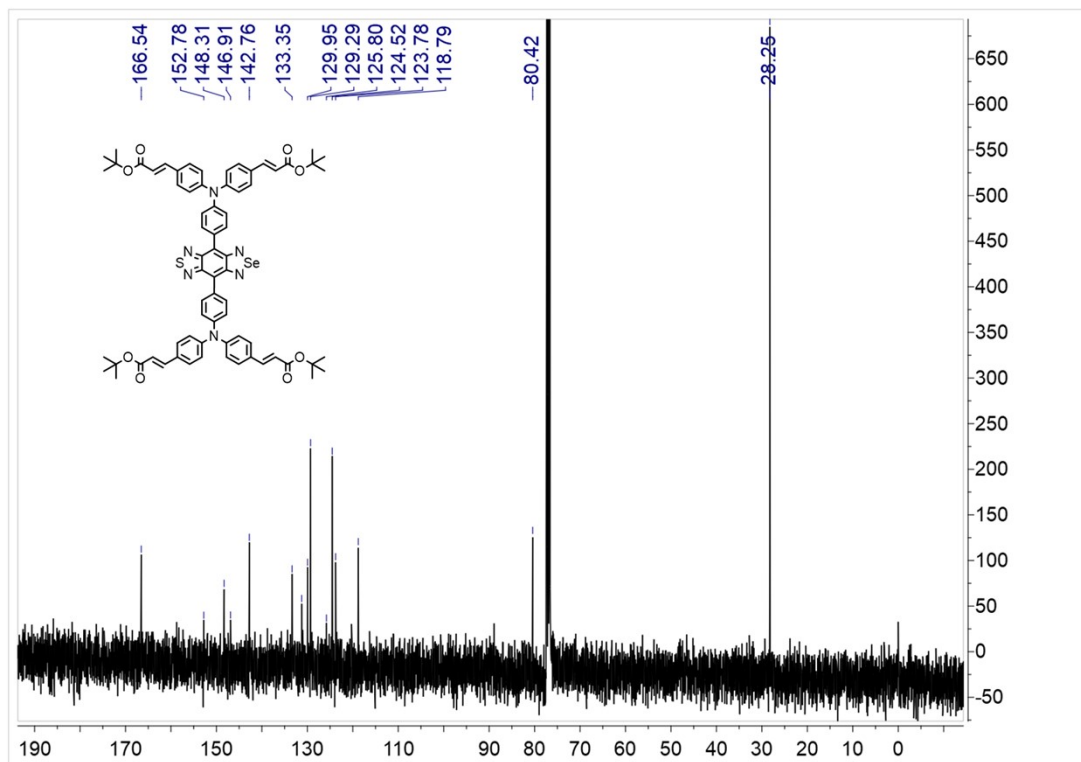


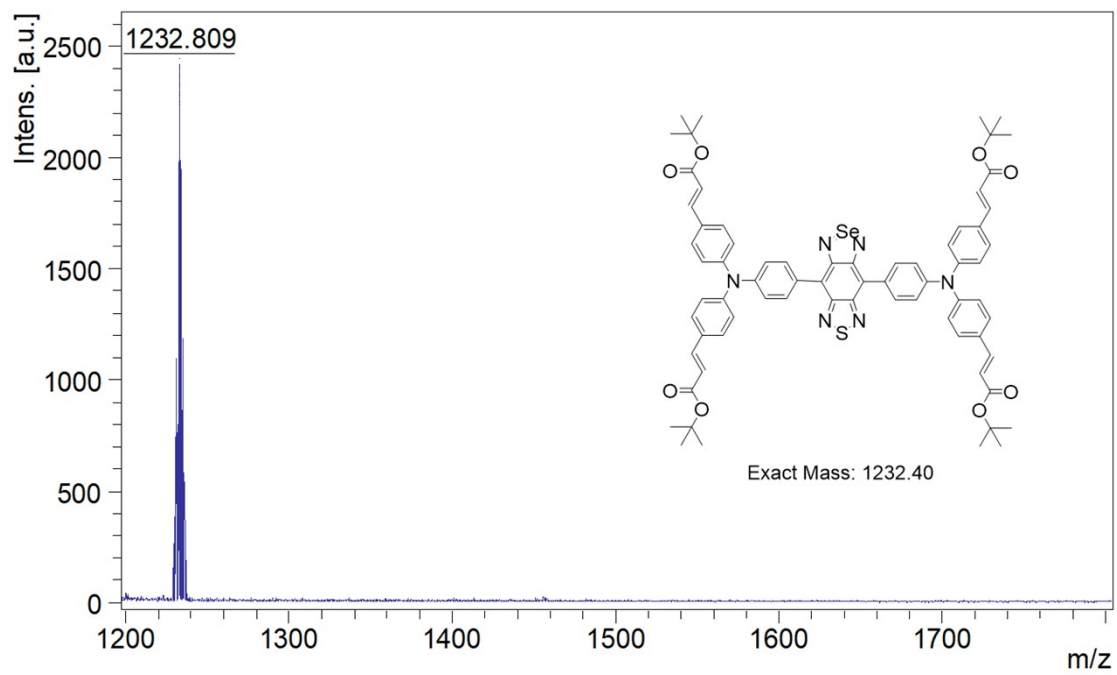












## References

1. S. Y. B. Wang, X. Chai, T. Li, Q. Wu, T. Wang, *Chem. Eur. J.* , 2016, **22**, 5649-5656.
2. T. S. C. Li, X. Li, Z. Xie, *ACS Appl. Nano Mater.*, 2022, **5**, 18691–18696.
3. L. Lei, F. Y, X. Meng, L. Xu, P. Liang, Y. Ma, Z. Dong, Y. Wang, X. B. Zhang, G. Song, *J. Am. Chem. Soc.*, 2023, **145**, 24386–24400.
4. L. Teng, G. S. Y. Liu, X. Han, Z. Li, Y. Wang, S. Huan, X. B. Zhang, W. Tan, *J. Am. Chem. Soc.* , 2019, **141**, 13572–13581.
5. P. Xiao, M. Liang, S. Yang, Y. Sun, J. Li, Z. Gu, L. Zhang, Q. Fan, X. Jiang, W. Wu, *Biomaterials*. 2023, 294, 121993.
6. F. Bai, W. Du, X. Liu, L. Su, Z. Li, T. Chen, X. Ge, Q. Li, H. Yang, J. Song, *Anal. Chem.* 2021, 93, 15279-15287.
7. J. Liu , Y. Tang , R. Wang , X. Wang , M. Fu , M. Zhang, F. Lu, Q. Fan, Q. Wang, *Sens. Actuators B Chem.* 2024, 414, 135951.